A Study of the Triggering Mechanism of a Trapatt Oscillator

by

Yvon Depratto

Submitted in partial fulfillment

of the requirements for the degree

of Master of Applied Science

Department of Electrical Engineering

Faculty of Science and Engineering

University of Ottawa

Ottawa, Canada

1974

Acknowledgements

I wish to express my appreciation and gratitude to Doctor W.J.R. Hoefer for his encouragement and his assistance during the elaboration of this work. I would also like to thank him for the helpful discussions we had during the completion of the report presented here.

I am much obliged to Doctor W.J. Chudobiak of the Communications Research Centre in Ottawa to have facilitated me the access to CRC Microwave Laboratories and to have allow me to profit of his vast knowledge and experience of the TRAPATT oscillator.

Finally, I wish to thank my wife, Cecile, for her patience and effort in typing this report.

ABSTRACT

The high efficiency mode of oscillation in avalanche diodes (TRAPATT-mode) has been studied extensively in recent years. Most authors agree basically on the theory of the steady state of such oscillations, but there exist different theories and observations concerning the initiation of the high efficiency mode, i.e. the process in which the current density in the diode rises to a value necessary to launch an avalanche shock front into the depletion region.

Three different starting mechanisms have been reported to date:

i - The generation of voltage swings at the TRAPATT (π - transit angle) frequency by trapping the IMPATT oscillation in a high-Q cavity (15,27,24).

ii - The build up of space-charge independent transit-time oscillations of small transit-angle

iii - The direct launching of a shock front by application of a very steep voltage pulse to a diode, of which parasitic impedances have been minimized (15).

In this study, the triggering behavior of the low cost FD-300 TRAPATT diode has been investigated

in coaxial and microstrip circuits of the Evan's type. The purpose of this study was to determine the mechanisms which initiate the TRAPATT mode in this particular diode, and to identify the circuit parameters that govern the triggering process. No attempt has been made to modify the active part of the device itself, however, the role of package parasitics has been taken into consideration.

From the analysis of the observation made during the above experiments, it has been concluded that the IMPATT oscillations play no significant role in the triggering of the TRAPATT mode in this particular diode. The mode is efficiently triggered by a transit oscillation with a frequency close to the natural TRAPATT frequency of the diode. This triggering mechanism is enhanced by the diode parasitic series inductance which favours the transit oscillation in preventing the highest harmonics from inducing a premature avalanche.

Table of Content

List of Figures

List of Tables

INTRODUCTION

In April 1967, Prager, Chang and Weisbrod (50) reported anomalous high efficiency oscillations in an IMPATT silicon diode. Later, Johnston, Scharfetter and Bartelink (40) observed the same mode in a germanium diode. This new-high-efficiency mode was inconsistent with the IMPATT theory. A number of authors have developed theories which partially explain the physics of the high efficiency mode, now generally known as the TRAPATT (Trapped Plasma Avalanche Triggered Transit) mode. Also a variety of circuit or resonator criteria essential for the TRAPATT mode, have been elaborated. However, the results reported to date do not fully explain a number of important diode-circuit interaction phenomena, for example, the essential triggering mechanism requirement to establish steady state TRAPATT oscillation: in the prominent literature on TRAPATT oscillations, large IMPATT swings at frequencies higher than the fundamental TRAPATT frequency have been considered necessary for triggering the anomalous or high efficiency avalanche condition. For this reason, TRAPATT oscillators have been equipped with high Q resonant structures for IMPATT triggering (15, 27, 24, 40). However, several "self starting" TRAPATT circuits initiate oscillations without these structures and without the presence of large IMPATT swings during the

initial state of operation.

The purpose of this thesis is to study the triggering mechanism of these "self-starting" oscillations and to optimize the conditions for reliable triggering in connection with maximum efficiency in the steady state.

CHAPTER I

Triggering mechanisms of the TRAPATT mode

1.1 Literature survey of triggering mechanisms of the TRAPATT mode

In September 1968, Johnston, Scharfetter and Bartelink (40) observed anomalous high efficiency oscillations in an IMPATT germanium diode. They recorded waveforms for different low frequency modes of operation corresponding to different configurations of the RF circuit in which the diode was incorporated. The mode called the "high efficiency mode" by these authors, is today commonly referred to as the TRAPATT mode. The TRAPATT waveforms indicate that the oscillation begins in the normal IMPATT mode and gradually, as the amplitude builds up, transforms to a two-frequency component waveform. As this occurs, the IMPATT frequency is pulled to lower values while the high-efficiency load signal establishes itself at one-half the lowered IMPATT frequency. Measurements performed at lower frequencies indicate that very few cycles of IMPATT oscillations are needed to start the TRAPATT mode.

In February 1969, Hoefflinger, Snapp, and Stark (35) found another triggering mechanism for the high-efficiency mode. They had observed that TRAPATT diode circuit combinations could also operate as amplifiers when triggered by injecting an external signal. According to their experiments, an avalanche

shock front is triggered in the diode, once the injected signal exceeds the threshold value.

In September 1969, Clorfeine (15) presented a detailed theory for the TRAPATT steady state. He was of the opinion that IMPATT oscillations would in general provide the starting mechanism for the TRAPATT mode, but would not be required if a sufficiently fast rising initial current could be provided:

> *"It was reported that conventional transit-time oscillations appear to trigger the high-efficiency oscillatory state. Such would be expected on the basis of the theory presented here. If a current generator with sufficiently small rise time were available, then no additional starting mechanism would be required. In the absence of such generators, however, it is the transit-time oscillations that provide the rapid current increase necessary to trigger the high efficiency mode."*

He also added that the role of the transit-time oscillations in the steady state of the high-efficiency mode must not be interpreted as oscillations that trigger the plasma at each cycle, but as essential harmonics that serve the functions of wave shaping.

In December 1969, Evans (27), in his paper "Circuits for High-Efficiency Avalanche Diode Oscillators", went further in the description of the triggering mechanism by demonstrating the degeneration of the IMPATT mode into the TRAPATT when the former has reached a saturation level: ". . .the space charge is depressing

the field so that the carrier drift velocity may drop below saturation and some carriers may be trapped for a short time in the low field region". He concluded that to start the TRAPATT oscillations, very large IMPATT swings must exist across the diode.

In January 1970, R.J. Chaffin (9) reported in his letter that ". . .TRAPATT outputs were observed at 560 MHz and 840 MHz. The TRAPATT outputs were at the sixth and fourth subharmonics, respectively, of the IMPATT oscillations." Other authors have reported similar results for different diodes.

Having simulated the TRAPATT oscillation in a silicon avalanche diode on a computer, M. Malsumura and H. Abe (47) reported in November 1970 that a large IMPATT swing is not always necessary to trigger the mode. The diode waveforms were observed, in a circuit similar to that described by Evans, for various slug tuner sets and positions. The results indicate that ". . .the TRAPATT mode is generally, but not necessarily, triggered by large-signal oscillations of the IMPATT mode, and that the mode starts to oscillate easily when a period of the relaxation oscillation is approximately equal to the time lag of the circuit response." The purpose of these experiments was simply to observe the triggering waveforms as the tuners positions were varied. Improvement of the oscillator efficiency was not aimed by the authors.

At the same time, Evans (30) was of opinion that analytical treatments of the TRAPATT mode in avalanche diodes did not consider in sufficient detail the initial starting conditions for this mode. He examined this question in greater detail by analysing a number of diode structures using a large computer program.

> *"The results of these experiments have indicated that the requirements for efficient TRAPATT operation and the requirements for IMPATT operation diverge with increasing frequency. Since the IMPATT oscillation is required to start the TRAPATT mode, self-starting TRAPATT oscillators are increasingly difficult to fabricate as the operating frequency is increased."*

In order to eliminate the problem of decrease in efficiency, a new diode structure was proposed. "The new structure is asymmetric with a one side optimized for the IMPATT oscillations and the other side optimized for efficient TRAPATT operation." However, even with this improvement, the TRAPATT efficiency is limited at high frequencies. Evan's computer simulation is a very complete analysis of the diode parameters. This work could be very valuable to forecast experimental results on triggering mechanisms of TRAPATT oscillations.

Also in November 1970, Prager, Chang and Weisbrod (51) built an amplifier similar to that of Hoefflinger except that the input signal was exactly

at the resonance frequency of the diode circuit. In examining the frequency spectrum of the amplifier, they found that a mysterious frequency was present in the signal OFF condition. This frequency was not harmonically related to the fundamental and it was too low to agree with any normal transit-time calculation. The exact origin of this oscillation is still undiscovered.

In May 1971, Snapp (58) developed a technique to identify the triggering IMPATT frequency present in the spectrum of a TRAPATT oscillator. He used the variation of the detected envelope of the diode current due to the insertion of a band-stop at the IMPATT frequency into the detecting circuit. A detailed description of this technique will be given in Chapter 3.

1.2 Known efficient triggering mechanisms

According to TRAPATT steady-state theory, large IMPATT oscillations should trigger the high-efficiency mode (27, 24, 15). A triggering frequency is often reported by authors while describing the results they have obtained during experiments on the steady-state of the mode. They refer to it as the triggering IMPATT oscillation. In the oscillator used in their experiments, the IMPATT oscillation is emphasized greatly by providing resonant conditions at the IMPATT frequency. This enhancement is achieved

either by modifying the diode structure (30) or/and by adding reactive components to the external circuit (27). Hoefflinger discovered in his experiments on high-efficiency amplifiers that the TRAPATT mode can be started by injecting a signal at a frequency close to the avalanche resonance frequency into the diode. The generator providing the triggering signal plays the part of the IMPATT resonator in the free-running oscillator. Thus, whenever a signal is injected into the avalanche diode, the TRAPATT oscillators starts.

1.3 Purpose of the thesis

In Chudobiak's microstrip oscillator, (13) however, the triggering oscillation conditions seem to be satisfied whenever the TRAPATT requirements are met by the external circuit. In this self-starting oscillator, no external resonant circuit is provided for the IMPATT frequency.

The objective of this thesis is to study the TRAPATT triggering mechanism of the self-starting type. The study is first oriented towards the identification of the triggering oscillation and measurement of its frequency. Then, the circuit and diode parameters which affect the triggering mechanism of the TRAPATT oscillations are determined.

1.4 Methods employed to detect the triggering mechanisms

Different methods are employed to detect the triggering oscillation, to determine its frequency and the way in which it degenerates into the TRAPATT mode. The different methods used (Table 1.1) can be divided into two complementary approaches: the frequency domain approach and the time domain approach. The description of those methods and the obtained results are reported in chapters 3 and 4.

TABLE 1.1

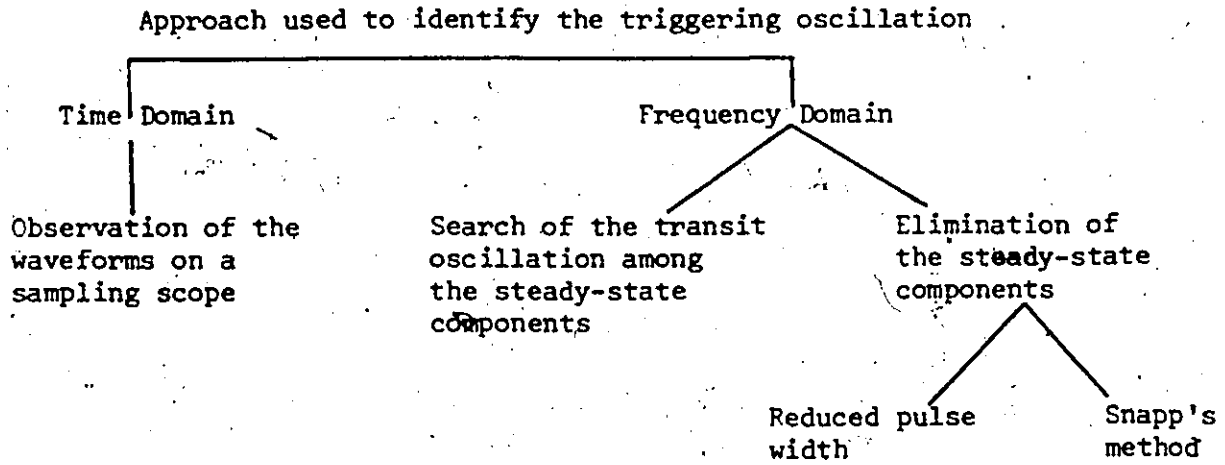

Once the triggering waveform and frequency are identified, it is possible to determine those circuit parameters which affect the triggering mechanism. The methods used to identify those parameters and the results

obtained during the experiments are described in Chapter 4. One possible procedure is to vary the parameters which are suspected to have an influence on the triggering mechanism. Among them are the quality of the line used in the circuit and the parasitic impedance of the diode package. Another method is to evaluate an equivalent circuit of the diode and to determine what relationship it bears with the triggering oscillation.

CHAPTER 2

The TRAPATT circuit

2.1 Different functions of the TRAPATT circuit

The purpose of the TRAPATT oscillator is the transformation of DC energy into RF energy. This DC energy can be supplied in a continuous or pulsed manner depending on the thermal limitations of the diode.

To generate and sustain a large RF oscillation, the TRAPATT circuit must fulfill two main functions. It must provide a fast rising pulse which will trigger the avalanche in the diode and it must allow the energy of the fundamental oscillation to flow outside the resonator structure.

The object of this section is to explain the different parts of the TRAPATT circuit. The description starts with the RF section which is the heart of the circuit. Then follows a description of the biasing Tee and of the power supply pulser which feeds the circuit. The block diagram of figure 2.1 shows the overall circuit with the TRAPATT resonator, the probes, the load, the biasing Tee and the power supply.

Figure 2.1: Block diagram of the TRAPATT circuit

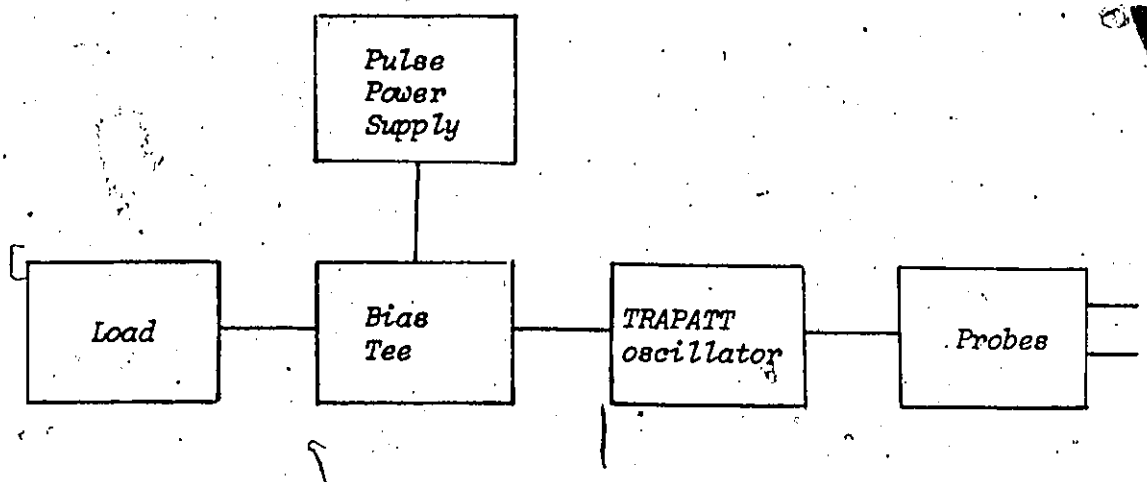

2.2 Description of the resonator

The resonator mechanism of the TRAPATT circuit is very simple (appendix 2). When the junction field collapses, the diode terminals voltage drops to almost zero. It results in a negative pulse which propagates on the transmission line towards the filter. The short circuit property of the low pass filter at harmonics frequencies causes the inversion and reflection of the negative pulse towards the diode. The reflected pulse has then a magnitude which is twice the breakdown value. At its incidence at the diode, which has recovered from the low voltage state, it triggers a new avalanche and

the cycle is repeated. The electrical length of the line between the diode and the filter determines the frequency of the oscillator by causing the wavelength delay of the triggering pulse.

The TRAPATT oscillator used in this work was of the type described by Evans. The equivalent circuit of the RF TRAPATT circuit is a half wavelength line terminated by a π section low-pass filter (figure 2.2). By its position on the line, the low pass filter input impedance almost equals the circuit input impedance.

Figure 2.2

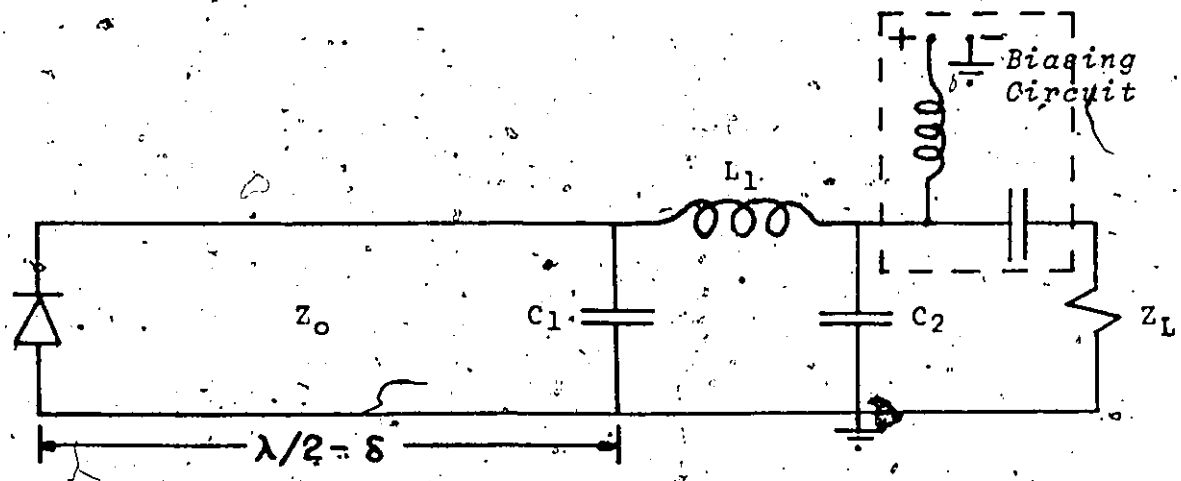

Equivalent circuit of the resonator presented at the diode

In the circuit (figure 2.3), the diode is mounted at one end of a 50 ohm line. At less than half a wavelength from it, tuners constitute the low pass filter. They are made of sections of low characteristic impedance transmission line. Their number can easily be reduced to two (or even one) if the required input impedance of the circuit is known.

Figure 2.3: RF TRAPATT oscillator

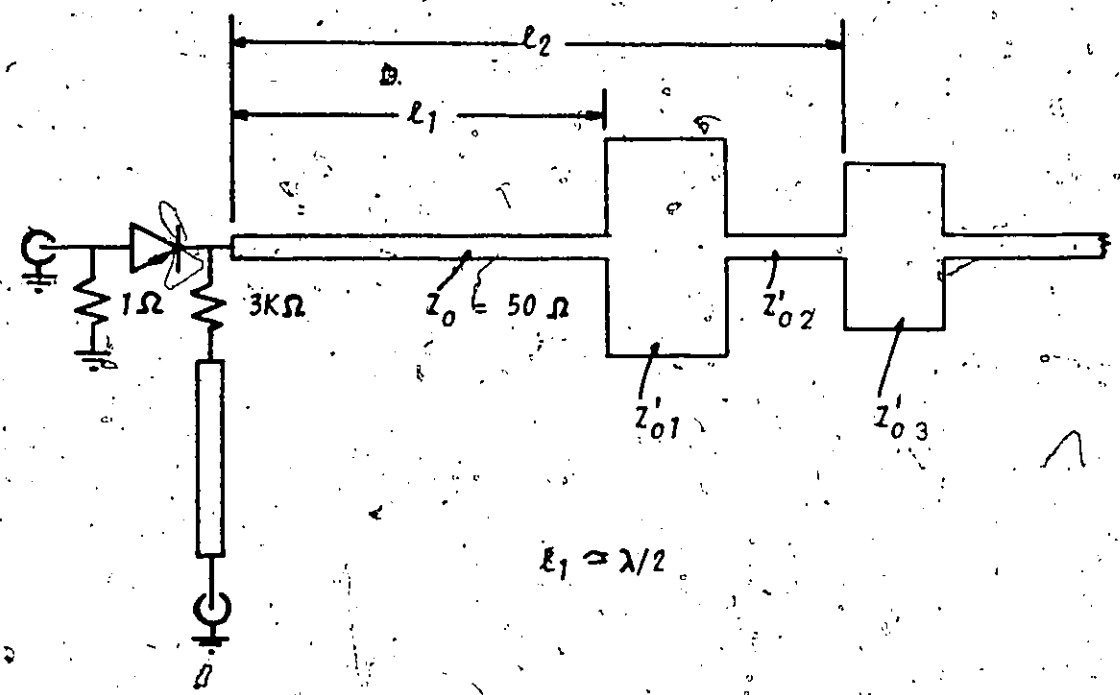

The capacitance C and the inductance L of the equivalent circuit can be determined by using a Smith immittance Chart

and the equation.

$$C = \frac{\ell}{Z'_{on}\, v_p} \quad \text{in Farad}$$

$$L = \frac{\ell\, Z'_{on}}{v_p} \quad \text{in Henry}$$

Where Z'_{on} is the characteristic impedance of the section of transmission line, v_p represents the phase velocity and ℓ is the length of the section (27).

A study of the standing wave pattern of the first three harmonics has shown that the filter behaves like a 50 ohm line at the fundamental and like a short circuit at higher frequencies (figures 2.4).

The positions of different sets of tuners chosen to obtain a maximum efficiency at different frequencies, are given in table 2.1. Also the characteristic impedance and the geometric dimensions of the different tuners used during this work are reported in table 2.2.

Table 2.1: Positions of tuners to obtain maximum efficiency at different frequencies

	Frequency in MHz	*Tuner identification*	*Position cm*
In the microstrip oscillation	330	B5	17.75
		B1	23.7
	690	B1	8.1
		A2	10.6
	830	B1	6.4
		B7	8.5
	1050	B1	5.1
		B7'	6.85
	1500	B2	2.85
		B4	5.10
		B6'	7.13
In the air-line oscillator	1500	C	7.73
		D	9.73
		D	11.53

Table 2.2: Description of the different tuners

Microstrip Type

Tuner identification	*Width cm*	$\frac{W}{h}$	Z_o *in ohm*	$\frac{\lambda_o}{\lambda_m}$	*Physical length of tuner cm*	*Free Space length cm*
A1	2.0	12.6	8.18	3.08	1.0	3.08
B1	2.6	16.4	6.48	3.12	1.0	3.12
B2	1.4	8.8	11.1	3.03	1.0	3.03
B3	0.9	5.7	16.0	2.83	0.8	2.27
B3'	0.8	5.0	17.5	2.82	0.9	2.54
B4	0.9	5.7	16.0	2.83	0.8	2.27
B5	2.55	16.1	6.61	3.10	1.4	4.35
B6	0.45	2.8	25.4	2.76	0.7	1.93
B7	1.35	8.5	11.8	2.98	0.85	2.54
B7'	1.4	8.8	11.2	3.03	0.95	2.88
B8	0.9	5.7	16.0	2.83	0.8	2.27
B8'	0.6	3.8	21.9	2.81	0.8	2.25

The relative dielectric constant = 9.8

The thickness of the substrate = 0.0625" (0.159 cm)

The microstrip equation are given in appendix 3

Air-line tuner

Tuner identification	*Outside diameter cm*	*Inside diameter cm*	*Length cm*	Z_o *ohm**
A	1.43	0.67	2.22	3.64
B	1.43	0.67	1.83	3.64
C	1.43	0.67	1.35	3.64
D	1.43	0.67	1.03	3.64

Center conductor diameter = 0.25"

2.3 Voltage and current probes

In order to observe the voltage and current waveforms without disturbing the oscillations, two probes were inserted at the diode in the oscillator.

The voltage probe consisted of a 3kΩ precision resistor (Pyrofilm corp. 62 -375) connecting the cathode of the diode to the 50Ω line leading to the instruments. The attenuation of the probe was nearly constant with frequency (figure 2.5). Hence, the voltage waveform transmitted by this probe was a good replica of the voltage at the diode.

A one ohm disc resistor (59) mounted between the diode and the ground plane constituted the current probe. The disc resistor was connected to an O.S.M.

*This is the calculated characteristic impedance. The measured value, using the T.D.R., is close to 8 ohms.

Figure 2.4
Voltage standing wave pattern between the first tuner and the diode

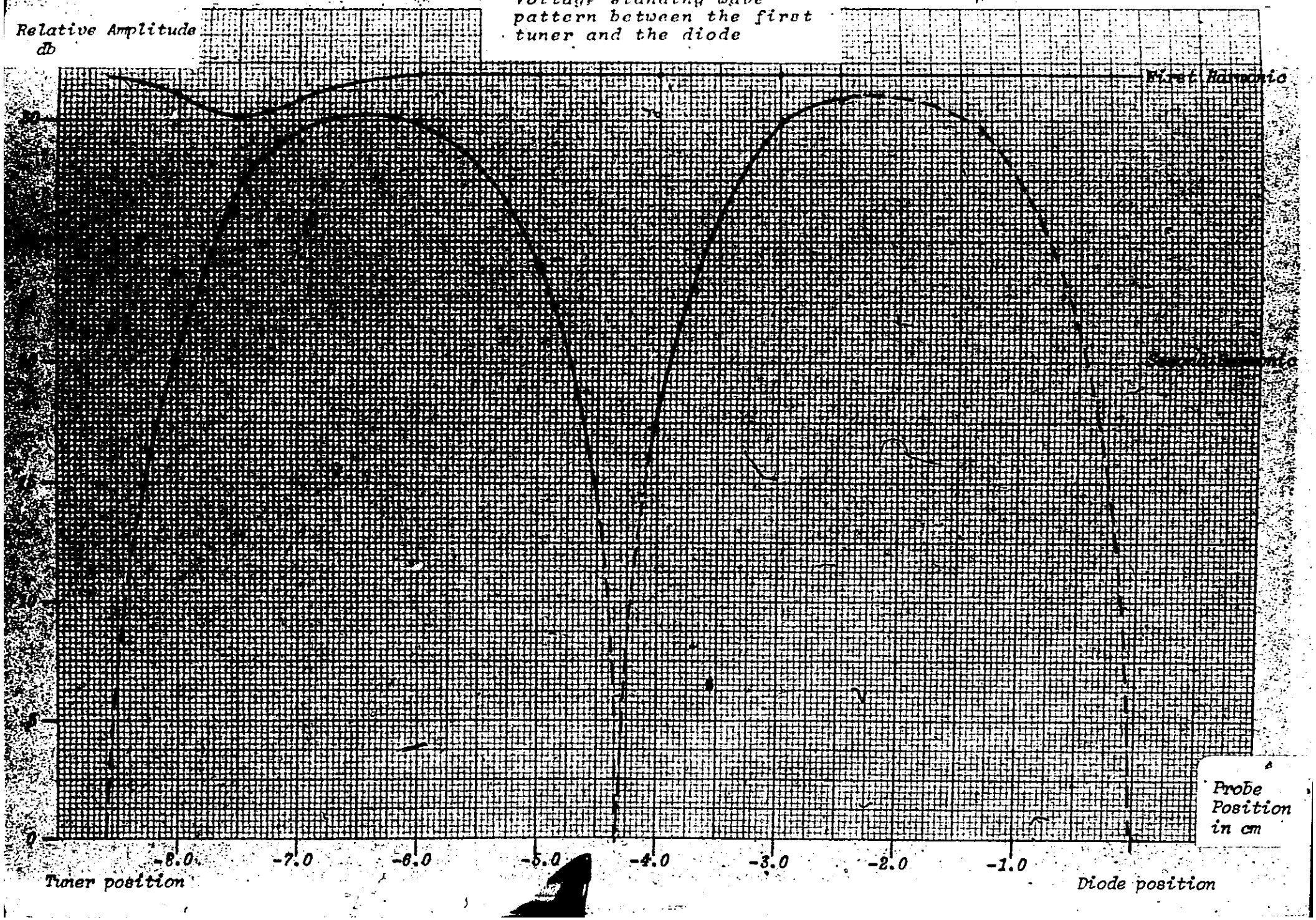

Figure 2.4
Voltage standing wave pattern between the first tuner and the diode

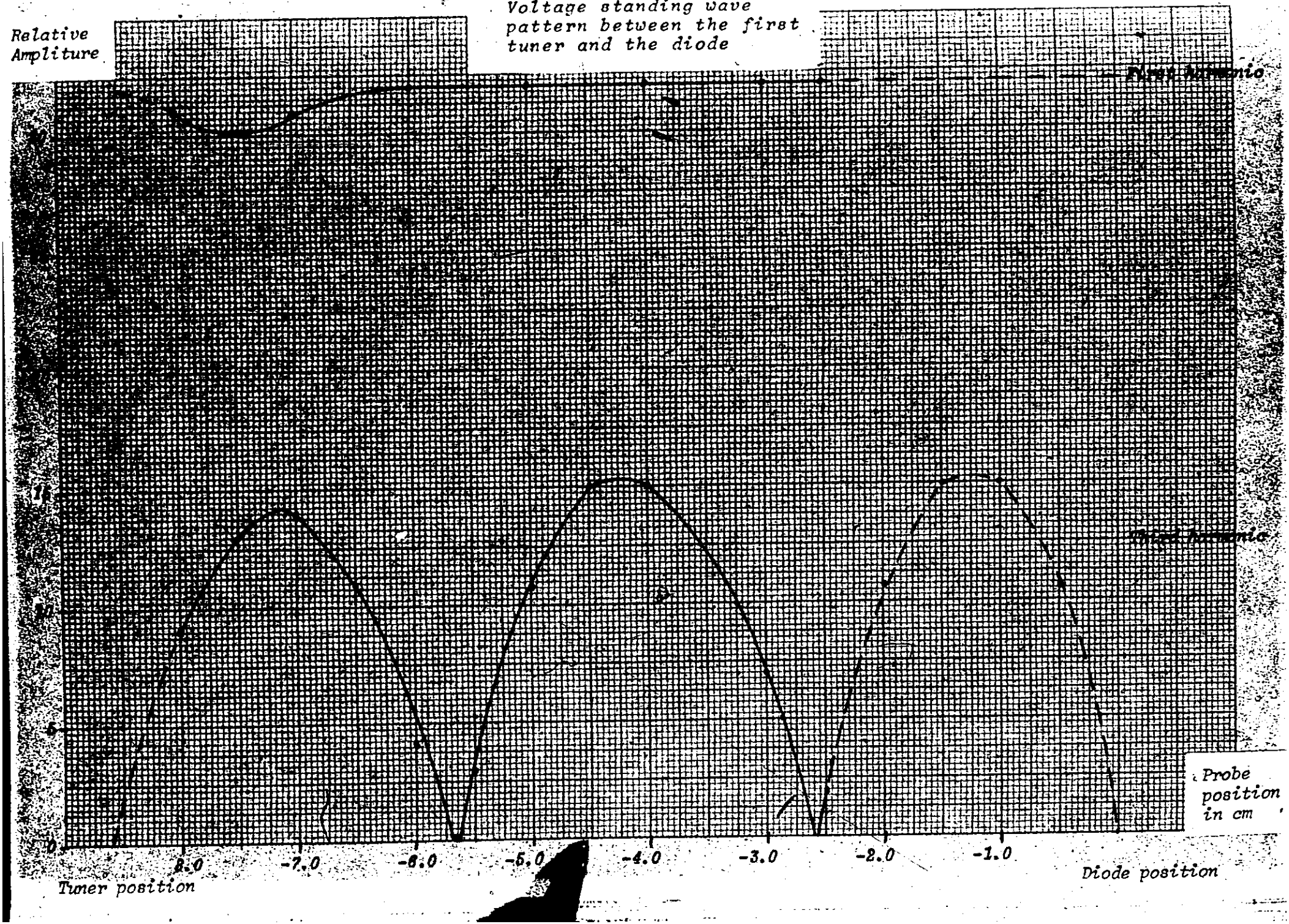

Figure 2.5
Attenuation of the voltage probe as a function of frequency

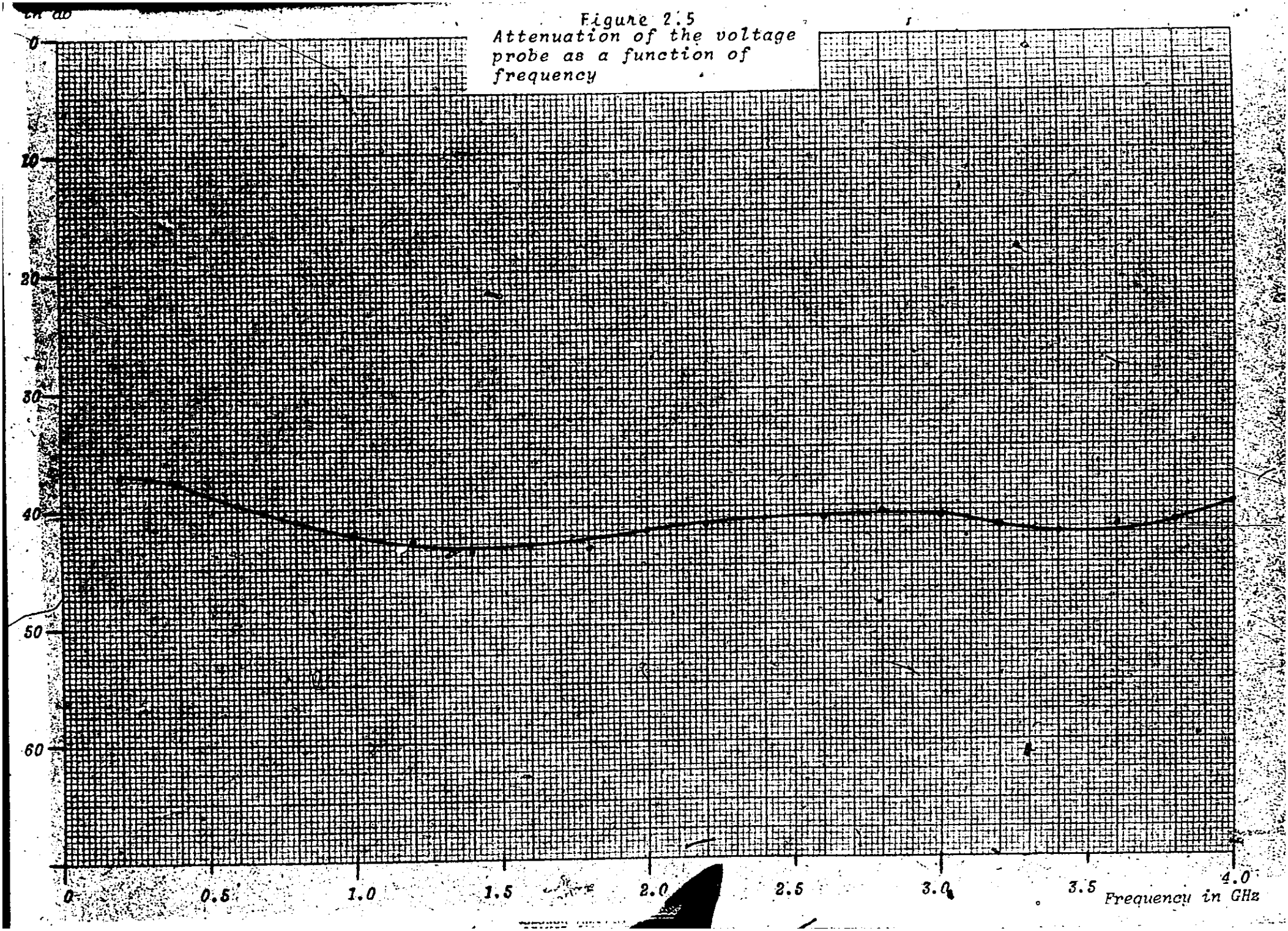

Figure 2.6 : Mounting of the one ohm disc resistor

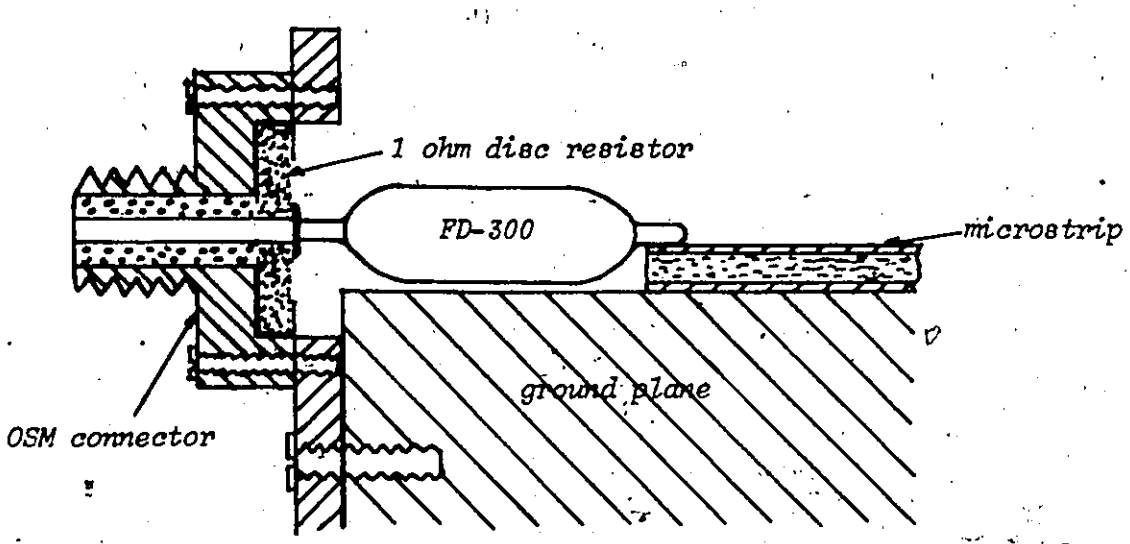

connector (figure 2.6) so that the oscillation was perturbed as little as possible. The voltage appearing at the terminals of the resistor and the connector was thus proportional to the current flowing in the diode.

2.4 The load

To verify the performance and the efficiency of the TRAPATT oscillator, the fundamental oscillation had to be measured and dissipated in a load. The power generated by the oscillator was first filtered through a low pass filter which rejected all higher residual harmonics. A 20db directional coupler allowed the monitoring of the fundamental frequency with a spectrum analyser or a crystal detector. Then, the output signal of the directional coupler was dissipated in the thermistor of a power meter.

Figure 2.7: Bias Tee circuit

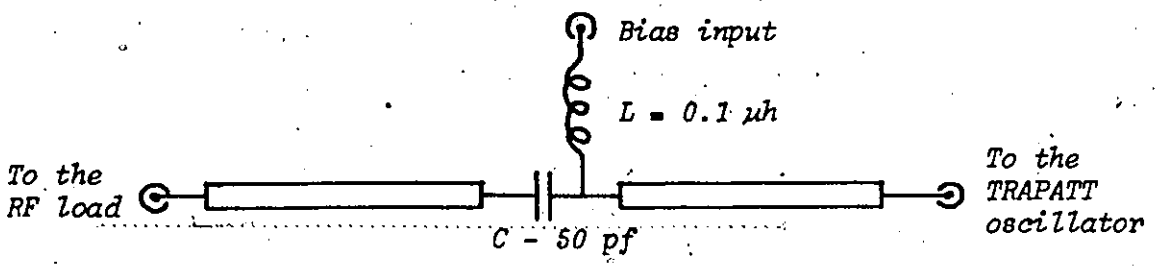

2.5 The bias tee

The bias tee consisted of a DC blocking capacitor and of a RF choke inductor as shown in (figure 2.7). The blocking capacitance was a 50 pf ATC capacitor. Its capacity was large enough not to attenuate the fundamental oscillation but small enough to sufficiently isolate the pulsed power supply from the RF load. The 0.1 μH inductance isolated the power supply from the RF signal without affecting significantly the rise and fall time of the biasing pulses. Bias currents of 1.25 to 1.5 amperes with a voltage of 300 volts were used to supply the oscillator.

2.6 The power supply pulser

The DC energy required at the bias input of

the oscillator was supplied through a pulser designed by W.J. Chudobiak and R. Burrill (14). This solid state pulse bias source was capable of output voltage up to 300 volts, and of peak output pulse currents in excess of 4 amperes. The pulse width was continuously variable in the range of 50 to 500 nanosecondes.

CHAPTER 3

The search for a triggering IMPATT oscillation

3.1 The IMPATT frequency of the FD-300

As mentioned in the previous chapter, many authors have reported that large IMPATT swings trigger the avalanche shock front in self-starting oscillators. Chaffin and Nisse (7,8) have detected, in the spectrum of an FD-300 diode operating in a TRAPATT circuit, a harmonic component around 3.6 GHz which they have identified as an IMPATT oscillation. The natural IMPATT frequency (π transit-angle) of the FD-300 is found, according to Read's theory, to be in the vicinity of

$$f_{IMPATT} = \frac{v_{ns}}{2W_c} = \frac{10^7 \text{ cm/sec}}{2 \times 10^{-3} \text{cm}} = 5 \text{ GHz}$$

where v_{ns} is the saturated velocity of the carriers

W_c is the depletion width in the diode

In order to evaluate the exact role that an IMPATT oscillation plays in the triggering of the TRAPATT mode, several measurements were made in the frequency and time domain, i.e., the frequency and the amplitude of the IMPATT oscillation as well as the interval in time during which it is present in the output spectrum were determined.

3.2 TRAPATT oscillator spectrum analysis

This method is the most simple approach to finding the triggering oscillation in the spectrum of a pulsed TRAPATT diode.

When the spectrum of a pulsed self-starting oscillator (the diode is a FD-300) was searched, only harmonics of the fundamental frequency could be detected on a spectrum analyser. Two possible explanations could be given for this result: either the triggering oscillations coincided with one of the harmonic of the TRAPATT oscillation, or they were hidden in the noise of the oscillator.

3.3 Reduced pulse width method

Since the triggering mechanism occurs before the TRAPATT steady-state oscillations, it is possible to eliminate the steady-state and to limit the oscillations to the triggering phase by reducing the biasing pulse width. Under those conditions, the triggering oscillation should be the only oscillation present in the spectrum and should not be affected by the reduction in pulse width. The frequency could then be determined simply with a spectrum analyser.

It was hoped that with this approach the initial triggering oscillation could be separated from the spectrum and the noise of the steady-state. The impedance of the TRAPATT circuit which was

tuned for a given frequency, was first adjusted such that a conjugate complex match between load and diode was established in order to obtain maximum output power. The steady-state oscillations were then suppressed by reducing the biasing pulse width until the fundamental frequency had disappeared from the spectrum of the diode voltage. Then the remaining oscillation was identified with a spectrum analyser.

The experiment has been carried out on several diodes and at several TRAPATT frequencies. The detected spectral components corresponding to different TRAPATT tunings are presented in table 3.1. Their frequencies depended more on the choice of the diode than on the tuning of the TRAPATT circuit. During the experiments, it was noted that the amplitude of the initial oscillation found in a given oscillator increased as the TRAPATT frequency was raised. However, the amplitude decreased rapidly as the tuner which controlled the TRAPATT frequency was close to the diode.

It must be noted that in reducing the pulse width, the conditions for triggering were slightly changed: the voltage rise time increased due to a reduced power dissipation in the output transistors of the pulser. Consequently, the current rise time was not the same for short and long pulses. (Compare the upper traces in figures 3.3a and 3.4a).

After measuring the frequency of the signal

emitted by the diode, biased with a short pulse, the experiment was carried out further. The biasing pulse width was increased in a stepwise manner to observe the behavior of the measured frequency as the TRAPATT mode was established. Figures 3.1 to 3.7 illustrate the components of the spectrum between 3 and 5 GHz for different pulse widths.

Figures 3.1 and 3.2 show the bias pulse waveforms at the diode. The pulse duration is so short that the mode cannot be established. Only the small initial oscillation is present in the output spectrum.

Table 3.1

Diode	*TRAPATT FREQUENCY in MHz*	*INITIAL OSCILLATION FREQ. in GHz*
A	330	4.18
	660	4.46
	889	4.2
	1050	4.2
B	630	4.24
C	330	3.8, 6.7
	690	5.9
D	330	3.4
	690	3.6
	990	3.6
E	330	4.6
	690	4.6
	990	5.0
F	330	3.0, 3.3
	690	2.8

Initial oscillation frequency for several TRAPATT frequencies and for several diodes

Under the biasing conditions of figure 3.3, the amplitude of the triggering oscillation is increased and the TRAPATT mode is initiated. In figure 3.4, the initial oscillation is completly hidden in the fifth harmonic (f = 3.4 GHz). Figures 3.6 show the current and voltage pulses of maximum length together with the corresponding spectrum between 3 and 5 GHz. This part of the spectrum seems to contain more components than the TRAPATT harmonics. This is explained by the fact that the circuit also produces a frequency half that of the fundamental frequency. The reflected pulse does not trigger the avalanche each time it is incident on the diode. The avalanche front can sweep the junction only after the arrival of the next reflection. This explains the presence of the 3060, 3740 and 4420 MHz components. The oscillations at 3600 and 4800 MHz are found to be spurious. Finally, figure 3.7 shows the (sin x/x) spectrum in the vicinity of the fundamental frequency.

3.4 Snapp's method

According to C. Snapp (58), the triggering process lasts for a very short interval of time and the corresponding detected current envelope is a spike of current which occurs just before the drop in the biasing voltage due to the onset of the TRAPATT mode. In inserting, between the circuit and the

detector, a high-pass filter with a cut-off frequency above the fundamental frequency, the triggering oscillation envelope can be observed. Then high-pass filters with higher and higher frequencies are used until the characteristic spike of the triggering oscillation disappears from the detected envelope. The frequency range, in which the transit oscillation occurs, is then delimited. Finally, this range is swept with a tunable bandpass filter to identify the exact frequency of the initial oscillation.

An experiment similar to that described by Snapp was carried out. A signal proportional to the diode current was obtained by detecting the voltage drop across a one ohm disc resistor connected in series with the diode. A back diode (O.S.M. model 20710) with a frequency range from 2 to 8 GHz was used as a detector when the back diode was terminated by a 200 ohm fed-through load. Its signal to noise ratio was of the order of 56db.

The moment at which the TRAPATT oscillation began was determined by detecting the voltage across the disc resistor through a 2 GHz low-pass filter (figure 3.8). For the delimitation of the frequency range of the initial oscillation, bandpass filters covering 4 to 8 GHz and 8 to 12 GHz respectively were employed instead of high-pass filters. The detected envelope of the signal passing through the 4 to 8 GHz bandpass filter started before the onset of the TRAPATT

Figure 3.1a) Average biasing voltage and current waveforms,
b) corresponding spectrum

a)

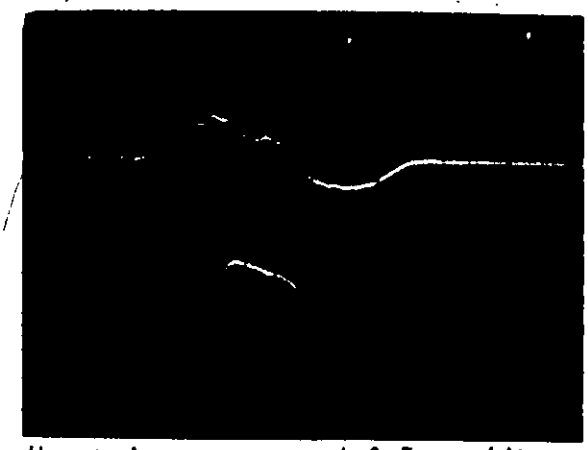

Upper trace: current-0.5 amp/div.
Lower trace: voltage=100 volt/div.
Horizontal : time =100 nsec/div.

b)

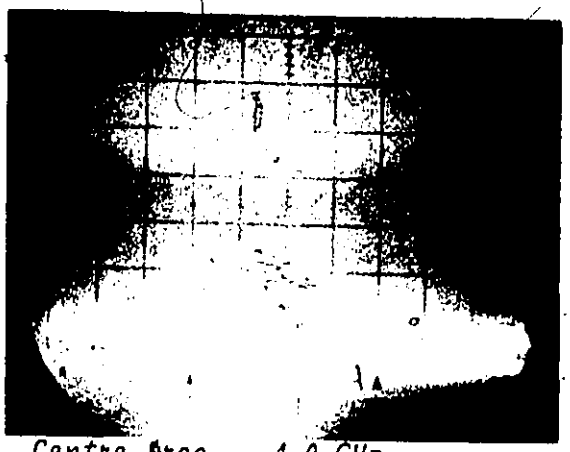

Centre freq. - 4.0 GHz
Width - 200 MHz /div.
Linear scale

Figure 3.2 a)

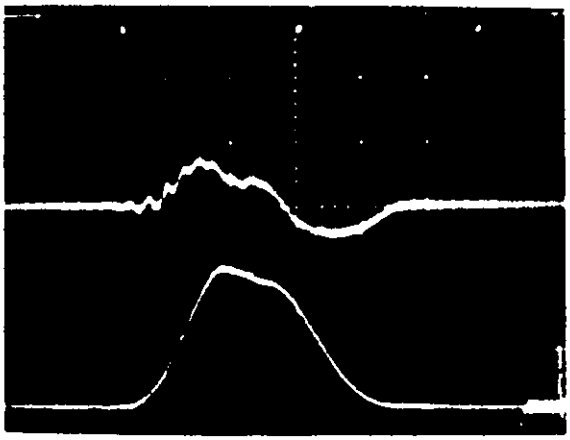

Upper trace: current -0.5 amp/div.
Lower trace: voltage -100 volt/div.
Horizontal : time -100 nsec/div.

Figure 3.2 b)

Centre freq. - 4.0 GHz
width - 200 MHz /div.
Linear scale

Figure 3.3 a)

Average biasing voltage and current waveforms

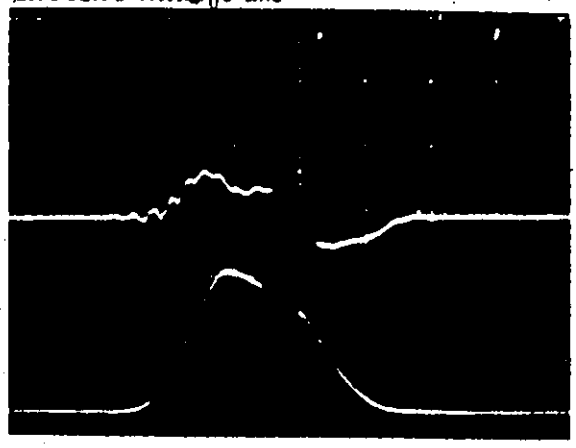

Upper trace: current=0.5 amp/div.
Lower trace: voltage=100 volt/div.
Horizontal scale =100 nsec/div.

Figure 3.3 b)

Corresponding spectrum

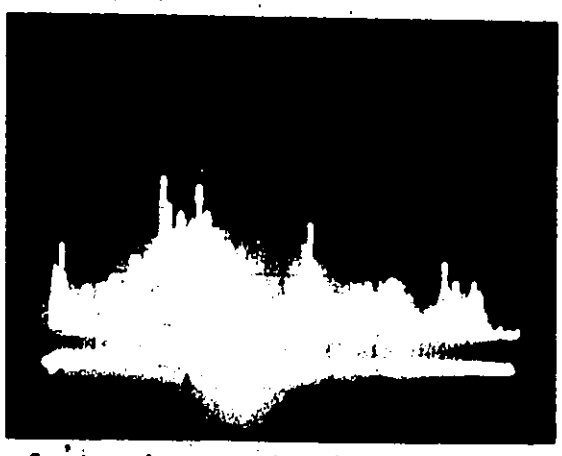

Centre freq. = 4.0 GHz
Width = 200 MHz /div.
Linear scale

Figure 3.4 a)

Average biasing voltage and current waveforms

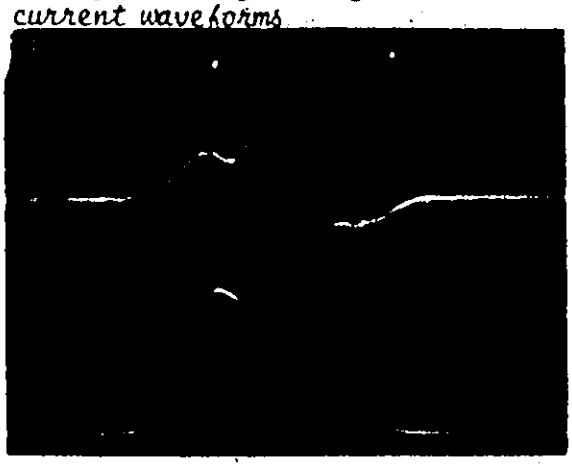

Upper trace: current=0.5 amp /div.
Lower trace: voltage=100 volt/div.
Horizontal scale =100 nsec/div.

Figure 3.4 b)

Corresponding spectrum

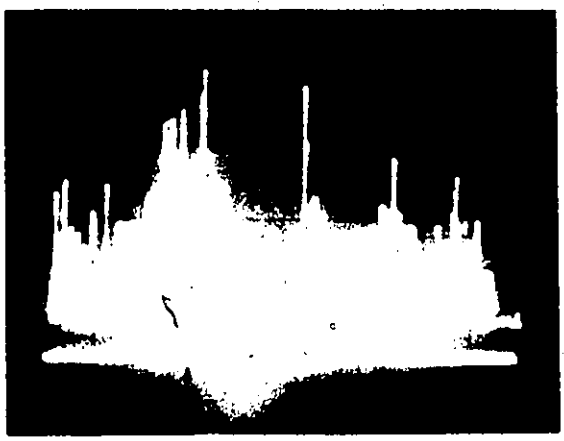

Centre freq. = 4.0 GHz
Width = 200 MHz /div.
Linear scale

oscillations (figure 3.9) while the envelope of the 8 to 12 GHz signal part began at the onset of the TRAPATT mode (figure 3.10). Thus, the initial oscillation was between 4 and 8 GHz. Finally, in order to identify the initial oscillation more precisely, this band was swept with a tunable bandpass filter. Figure 3.11 shows that the detected current increased before the drop in the input biasing voltage occured. The corresponding frequency was 4.2 GHz. It was harmonically related to the fundamental frequency.

Since this method used the fact that the triggering process must precede the TRAPATT oscillations, it was a repetition of the reduced pulse width method. Moreover, because the obtained results agreed with those of the previous experiment, Snapp's method was not carried out further.

The obtained results could not be considered to be very significant when compared with those of Snapp. He observed a clean envelope current spike of the triggering transit oscillation. The onset of the 4 to 8 GHz detected envelope (figure 3.9) was considered to represent the triggering oscillation, but the detected initial oscillation envelope at 4.2 GHz (figure 3.11) contributed only slightly to the total detected current. Moreover, since no component above 8 GHz appeared before the onset of the mode, the

Figure 3.5 a)
Average biasing voltage and current waveforms

Upper trace: current=0.5 amp/div.
Lower trace: voltage=100 volt/div.
Horizontal scale =100 nsec/div.

Figure 3.5 b)
Corresponding spectrum

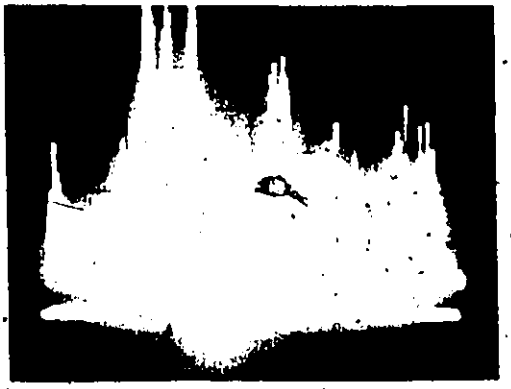

Centre freq. = 4.0 GHz
Width = 200 MHz /div.
Linear scale

Figure 3.6 a)
Average biasing voltage and current waveforms

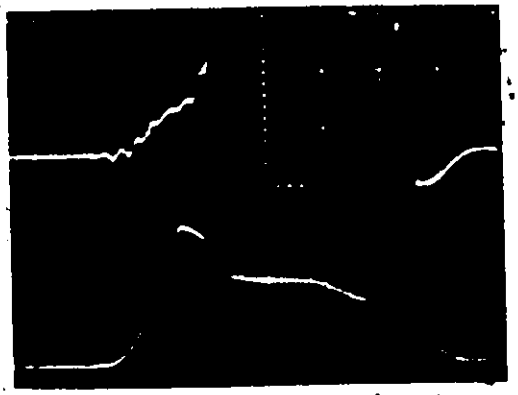

Upper trace: current =0.5 amp/div.
Lower trace: voltage =100 volt/div.
Horizontal scale =100 nsec/div.

Figure 3.6 b)
Corresponding spectrum

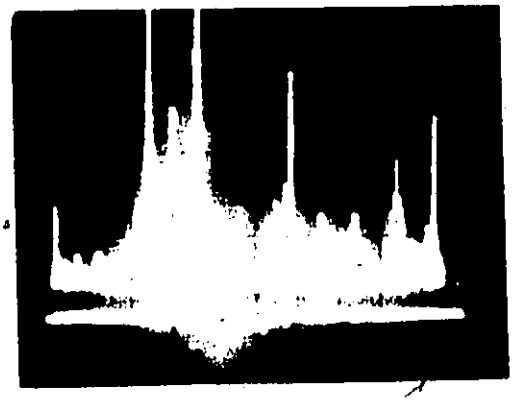

Centre freq. = 4.0 GHz
Width = 200 MHz /div.
Linear scale

Figure 3.7
TRAPATT output spectrum

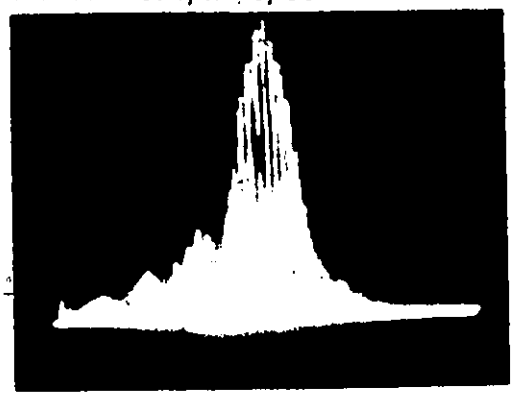

Centre freq. = 680 MHz
Width = 3 MHz /div.
Linear scale

Figure 3.8

The average biasing voltage and detected diode current (2 GHz low-pass filter)

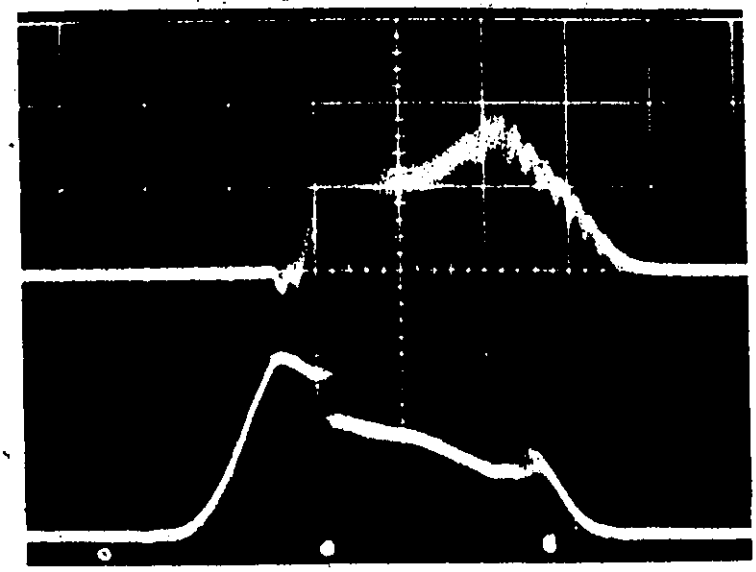

Upper trace: detected current

Lower trace: average biasing voltage

Lower scale = 100 volts /div.

Horizontal scale = 100 nsec /div.

Figure 3.9

The average biasing voltage and detected diode current (4-8 GHz band-pass filter)

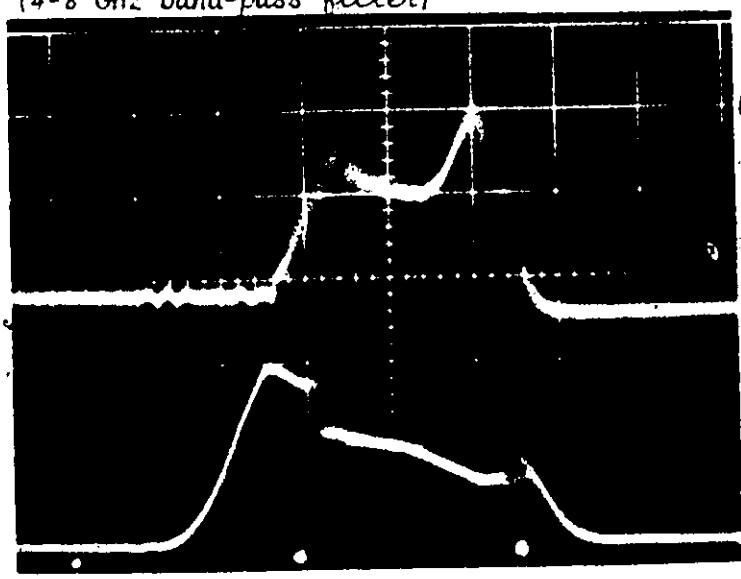

Upper trace: detected diode current

Lower trace: average biasing voltage

Lower scale = 100/div.

Horizontal scale = 100 nsec /div.

Figure 3.10

The average biasing voltage and detected diode current (8-12 GHz band-pass filter)

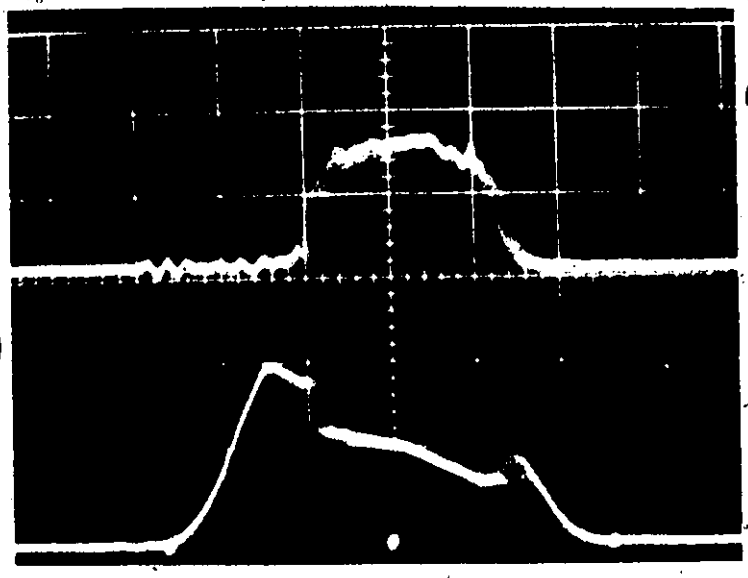

Upper trace: detected diode current through a 8-12 GHz band-pass filter.

Lower trace: average biasing voltage

Lower scale = 100 v/div.

Horizontal scale = 100 nsec /div.

Figure 3.11

The average biasing voltage and detected diode current (Tunable band-pass filter at 4.2 GHz)

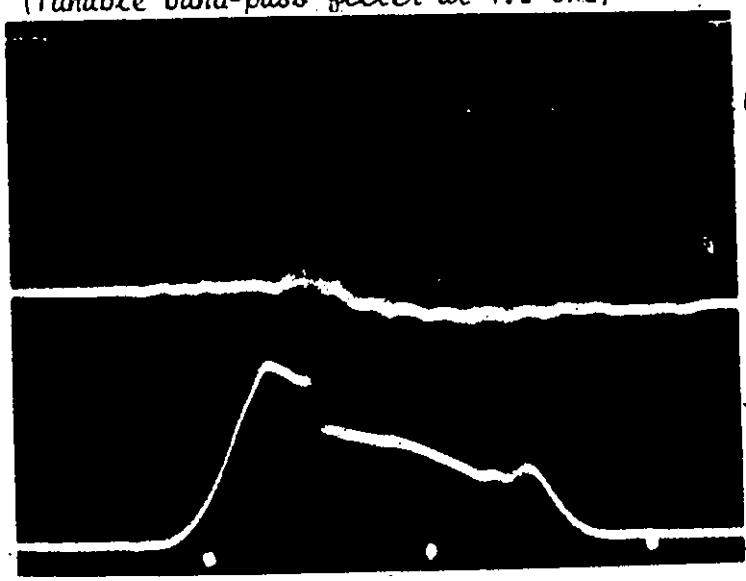

Upper trace: detected current envelope through the tunable band-pass filter at 4.2 GHz

Lower trace: average biasing voltage

Lower vert. scale = 100 v/div.

Horizontal scale = 100 nsec/div.

spectral components of the triggering oscillation had to be below that frequency.

3.5 The importance of the IMPATT oscillation

The search for the triggering IMPATT oscillation resulted in the identification of a small initial oscillation around 4 GHz. Its frequency was determined by the diode geometry and not by the external resonant circuit. However, the signal amplitude was so small (1 db above the noise level corresponding to a current density in the diode of about $0.1A/cm^2$) that no significant role could be attributed to the oscillation in the triggering of the avalanche shock front which requires $1700A/cm^2$.

The purpose of this section is to evaluate the importance of the initial oscillation in the triggering process. This is achieved by attenuating the 4 GHz initial oscillation in order to diminish its effect on the TRAPATT oscillation. If that high-frequency oscillation bears a direct relationship with the TRAPATT mode, then the triggering of the mode should become more and more difficult with increasing losses at 4-GHz.

This was verified by comparing the triggering behavior in two different oscillators. One involved a high-quality air-line (GR) in which the losses were low. The other circuit comprised a microstrip line

in which the dispersive effects were quite significant above 2 GHz, particularly for thick (h>50 mils) and high-dielectric constant ($e_r > 10$) substrates (38).

The experiment was performed at 1.5 GHz where the diode (FD-300) efficiency was low in the TRAPATT mode and where the proper adjustment of each parameter became critical. The results are reported in table 3.2

Table 3.2: *The average power at the fundamental frequency was measured with a power meter through a band-pass filter tuned to 1.5 GHz*

Diode Number	*Av. power in microstrip* mW	*Efficiency* η_m %	*Av. power in air-line* mW	*Efficiency* η_a %	$\frac{\eta_a - \eta_n}{\eta_a}$ %
71	0.96	1.76	1.25	2.2	2.0
67	0.94	1.72	1.24	2.27	2.4
66	0.31		0.37		
53	0.80	1.41	1.00	1.76	2.0

Where η_a is the efficiency in the air-line

η_m is the efficiency in the microstrip

The TRAPATT mode was initiated equally well in both circuits. However, the efficiency was lower in the microstrip oscillator. This was expected and can be ex-

plained in the following way. The harmonics of the TRAPATT frequency in the microstrip oscillator were attenuated and dispersed more than the fundamental. This, in turn, caused a reduction in the amplitude of the reflected pulse which triggered the avalanche in the diode. Hence, it resulted an oscillation mode which was less efficient than the oscillation in the air-line. Thus no important role is attributed to the initial oscillation at 4 GHz, even if it induced part of the negative resistance necessary to trigger the TRAPATT mode.

3.6 Conclusion

All the observations described in this chapter lead to the following conclusions:

- During the triggering period, a weak signal at about 4 GHz is present in the output spectrum of the oscillator.
- The frequency of this component is independent of the tuning of the resonant circuit, but it varies slightly from diode to diode.
- The amplitude of this component is too small (1 db above noise level) to launch an avalanche front which is characteristic of the TRAPATT mode.
- Even if the resonant circuit considerably attenuates the 4.0 GHz oscillation, the TRAPATT mode is easily triggered.

CHAPTER 4

Recording of transient TRAPATT waveforms

4.1 Introduction

In the search for an oscillation at the natural IMPATT frequency, a small oscillation at 4.0 GHz was detected before the establishment of the TRAPATT mode. However, its amplitude was so small that no significant role in the triggering of the avalanche shock front was attributed to this oscillation. The analysis of the diode voltage and current spectrums has thus failed to provide the necessary information required to understand the triggering mechanism of the TRAPATT mode.

A more direct approach, the recording of the diode waveforms, was required to visualize the triggering of the TRAPATT oscillation. The objective of studying the voltage and current waveforms is to obtain complementary information which could not be obtained in the frequency domain. In recording the diode oscillations, the frequency can be evaluated and it becomes possible to situate it in the time domain: how the first oscillation starts, how it grows and how it degenerates into TRAPATT oscillation.

4.2 Recording of the waveforms

The measurements and recordings were performed under the following conditions:

a) the TRAPATT circuit was tuned for maximum output power at the chosen frequency

b) the spectrum had (sin x/x) shape.

A stable drop in the biasing average voltage was also a good criterium of good performance.

To perform the experiment, a sampling scope with a bandwidth (12 GHz) broad enough to include the most important harmonics of the TRAPATT oscillation, was employed. Because the oscilloscope had to start sweeping before the beginning of the TRAPATT oscillation, an advanced triggering signal was needed. In order to obtain a jitter free display, the oscilloscope had to be triggered on the RF signal itself since the start of the RF waveform has a variable delay after the applied bias pulse. Furthermore, since the onset of the oscillation itself was to be displayed, the signal reaching the vertical input had to be delayed by 60 nanoseconds after the triggering signal.

The signal from the diode was divided, one part being directly fed into the triggering input, the other part reaching the sampling head after having travelled through a 100 foot RG 9/U cable (see figure 4.1). The disadvantage of this method was the increase in attenuation with frequency, leading to a distortion of the recorded waveform. (Figure 4.2 shows the attenuation of the line as a function of frequency). However

Figure 4.1

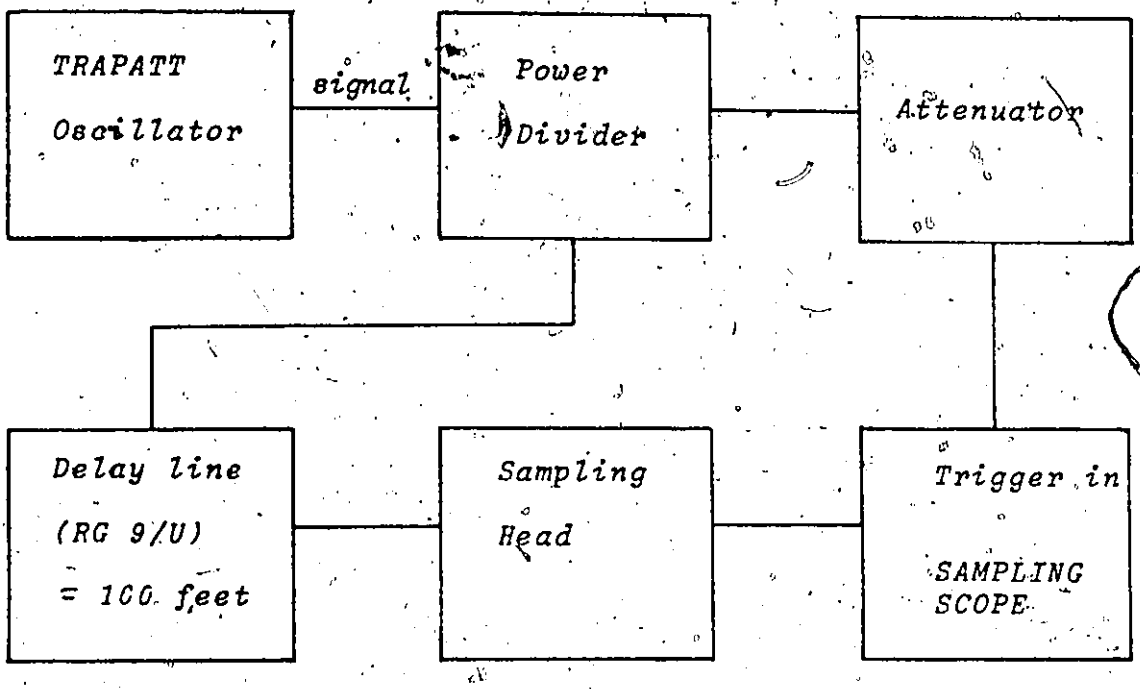

Figure 4.1: Set-up used to produce the jitter free waveforms

it was the only mean to achieve satisfactory resolution. An attempt to trigger the oscilloscope with an advanced triggering signal from the biasing pulser (see figure 4.3) resulted in a jumbled display.

Once all the conditions which assure a good performance of the TRAPATT oscillator and a jitter free display of the diode waveforms on the scope were met, the experiment was performed. The waveforms were recorded for different diodes and at different frequencies. Figures 4.4 to 4.9 show the recorded waveforms.

The recorded waveforms of figures 4.4-4.9 (mainly figure 4.4 show the different phases before the

Figure 4.2

Calibration of the Delay Line
Attenuation as a function of frequency

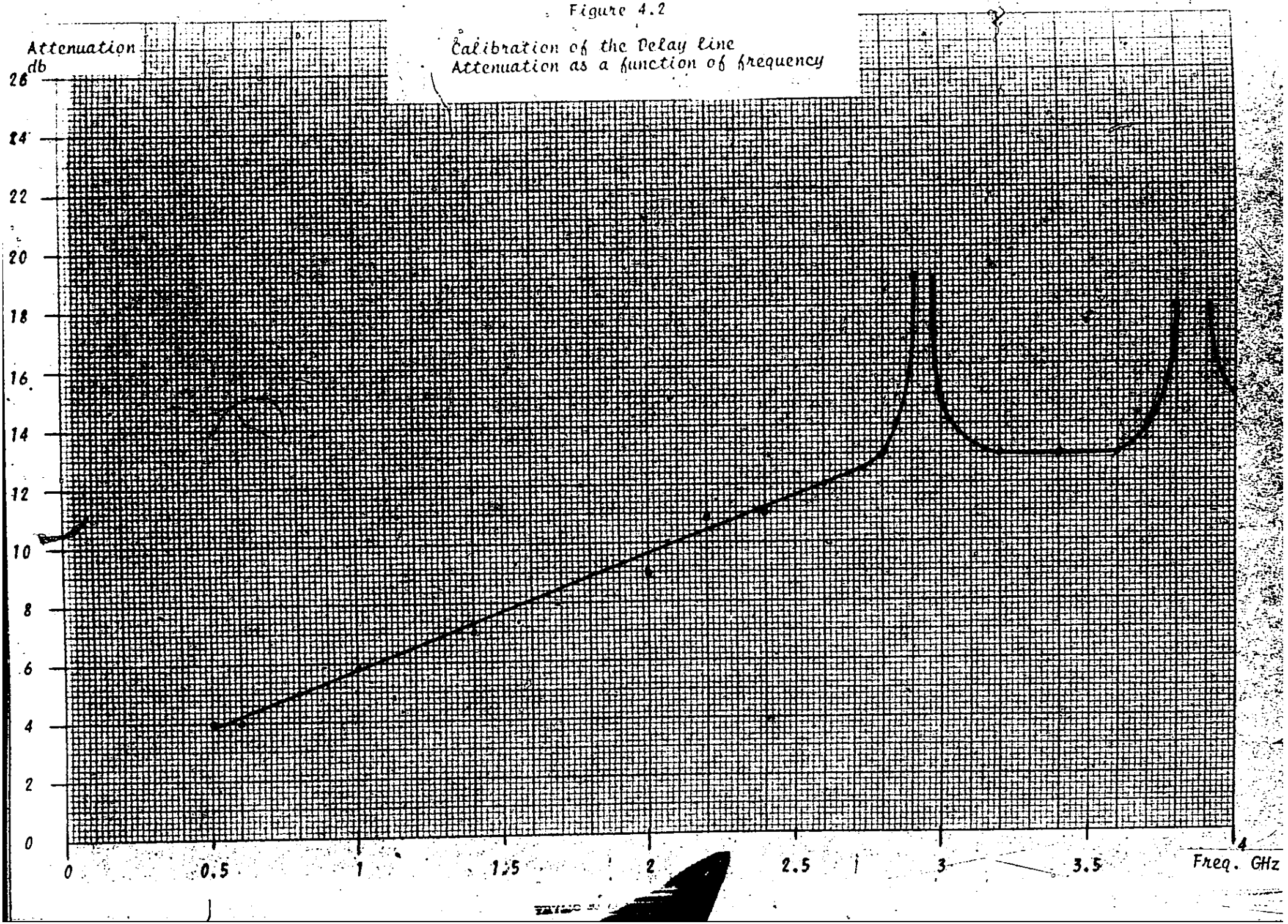

Figure 4.3

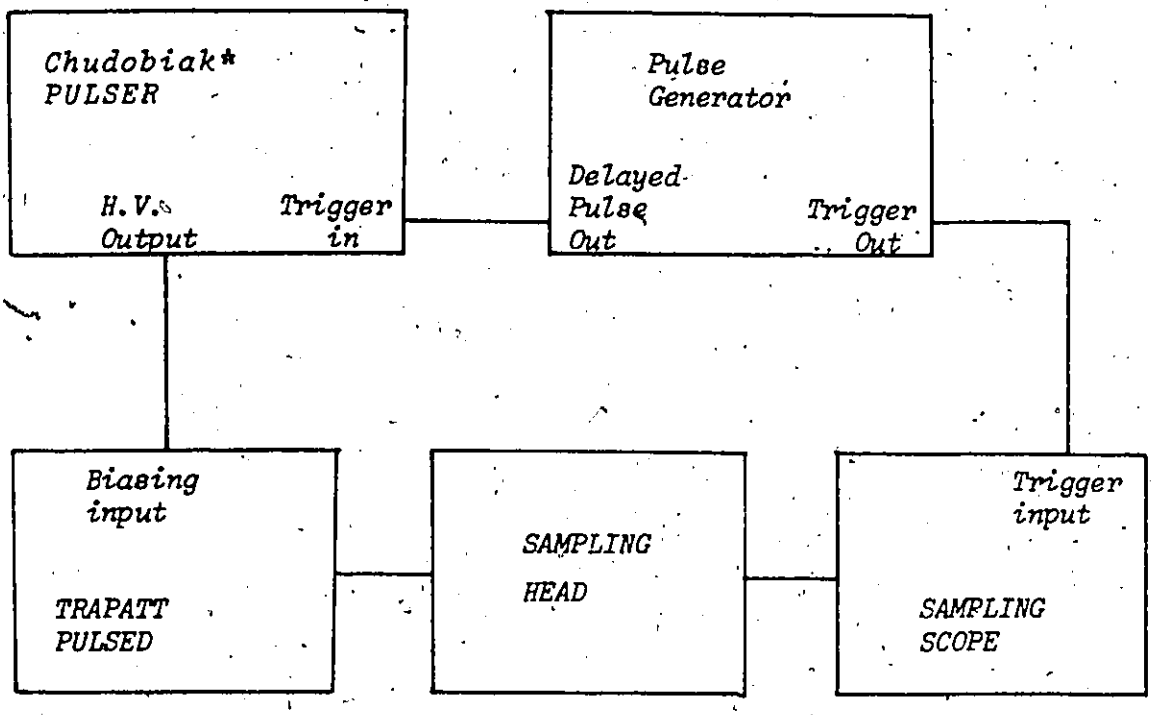

Figure 4.3: Set-up producing undistorded but jumbled waveforms.

establishment of the steady-state of the TRAPATT mode. First, the noise level increases as the diode reaches the breakdown point. Then after the value has been reached, a small oscillation, harmonically related to the fundamental frequency appears and grows exponentially until it is large enough to initiate the TRAPATT mode. At 330 and 400 MHz, the small oscillation is at twice the fundamental frequency. Above 400 MHz, it oscillates at the fundamental frequency and degenerates very rapidly into the TRAPATT mode. The last phase before the establishment of the TRAPATT mode in the

* *This pulser was designed by W.J. Chudobiak*

Figure 4.4
Voltage as a function of time (Freq = 330 MHz)

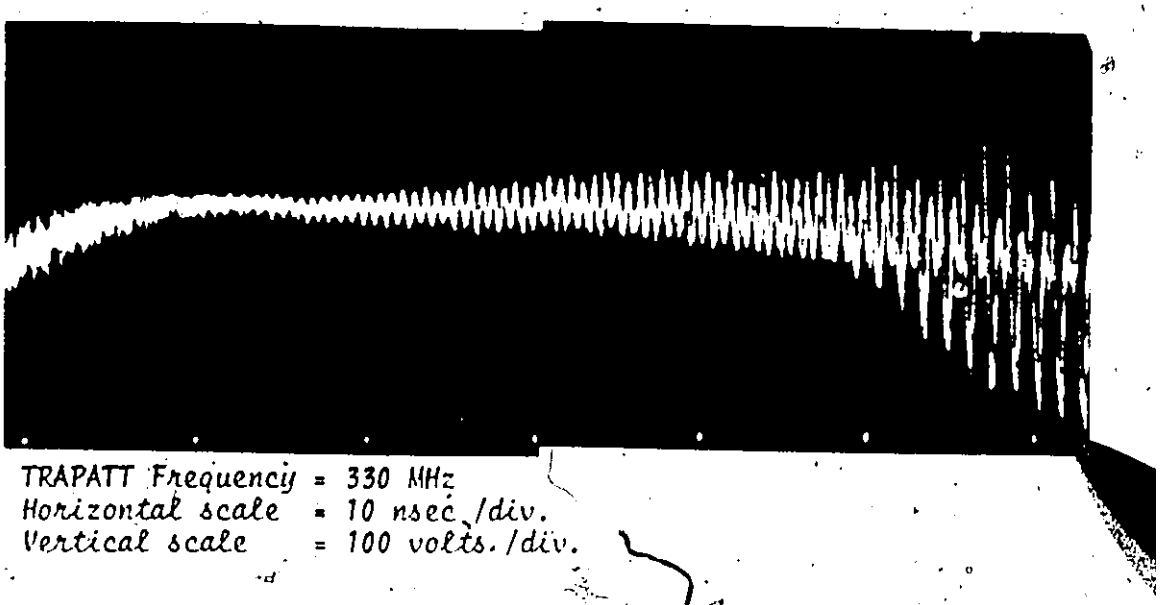

TRAPATT Frequency = 330 MHz
Horizontal scale = 10 nsec /div.
Vertical scale = 100 volts./div.

Figure 4.5
Voltage as a function of time (Freq. - 400 MHz)

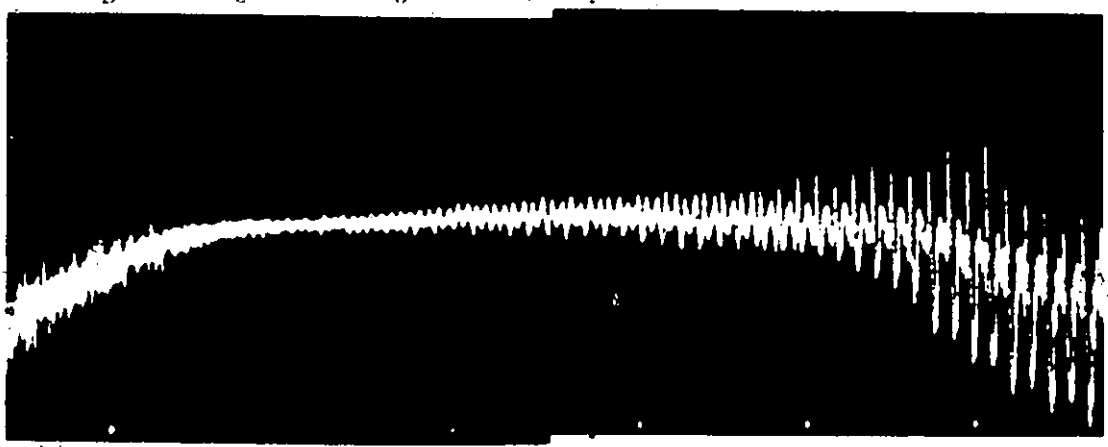

TRAPATT Frequency = 400 MHz
Horizontal scale = 10 nsec /div.
Vertical scale = 100 volt /div.

Figure 4.6 a)
Voltage as a function of time (Freq - 550 MHz)

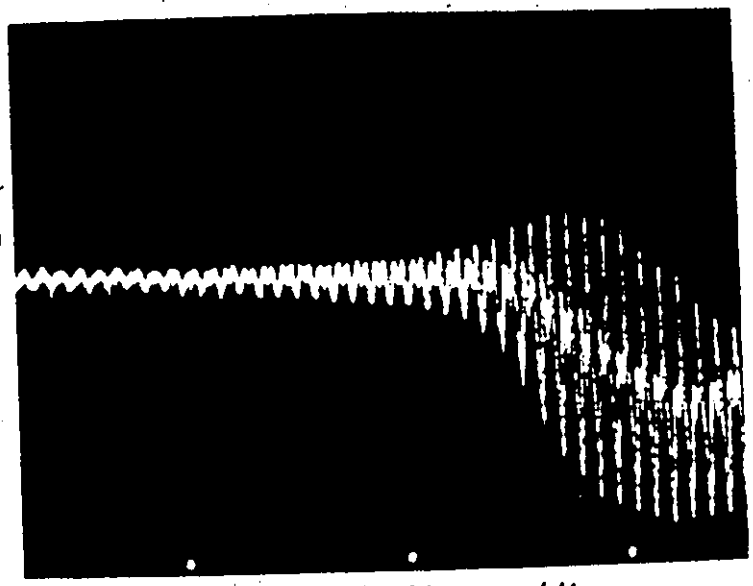

Horizontal : time = 10 nsec /div.
Vertical : voltage = 100 v/div.
= 58 db of att.

Figure ~~4.6 b~~)
Current as a function of time (Freq = 550 MHz)

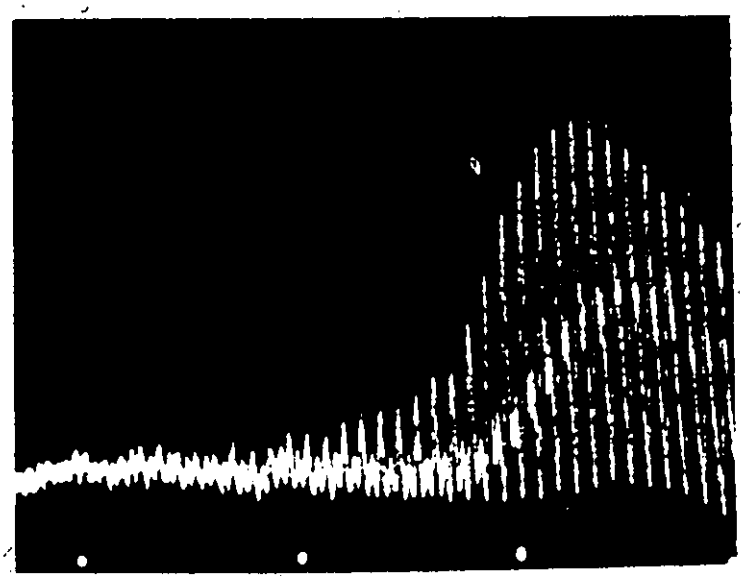

Horizontal scale - 10 nsec /div.
Vertical scale - 1 amp /div.

Figure 4.7

Voltage waveform (Freq. 660 MHz)
Horizontal scale: Time = 10 nsec/div.
Vertical scale: Voltage = 50V/div.
Biasing current = 1.5 amps

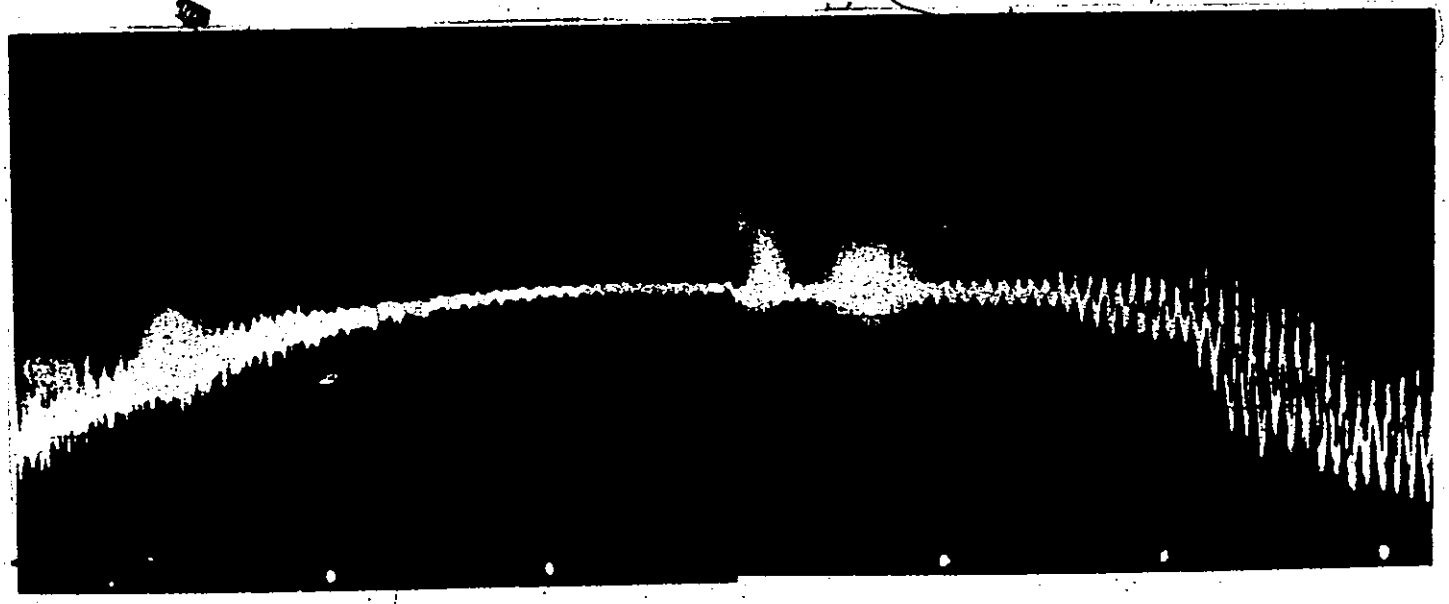

Figure 4.8 a)
Voltage waveform (Freq. 810 MHz)

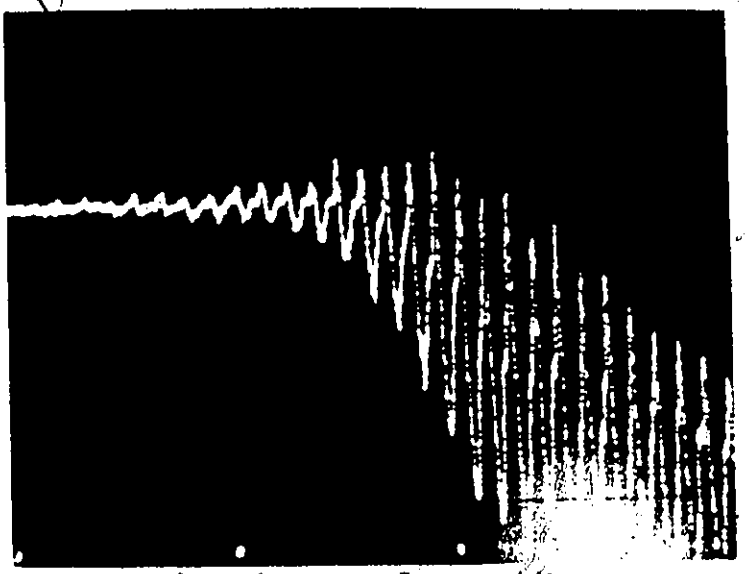

Horizontal : time = 5 nsec /div.
Vertical : voltage = the above scale

Figure 4.8 b)
Current waveform (Freq 810 MHz)

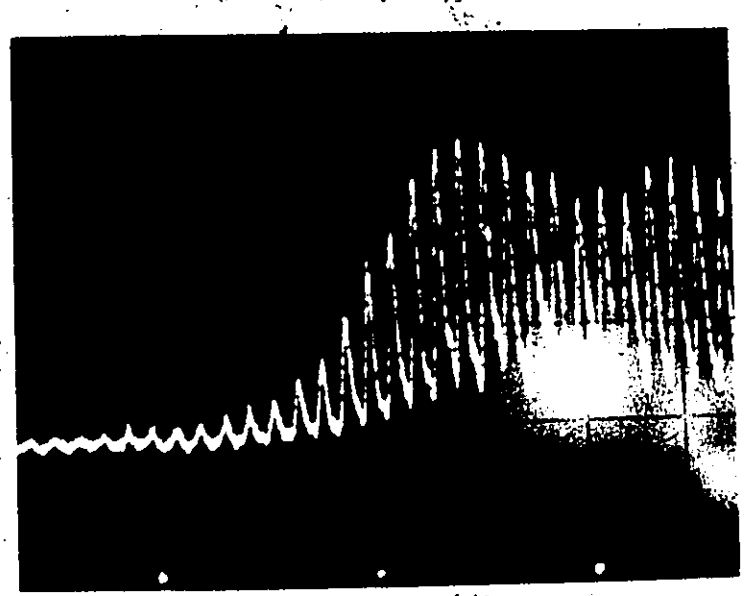

Horizontal time = 5 nsec /div.
Vertical current = 0.5 amp /div.

Figure 4.9 a)

Voltage waveforms when the frequency = 980 MHz

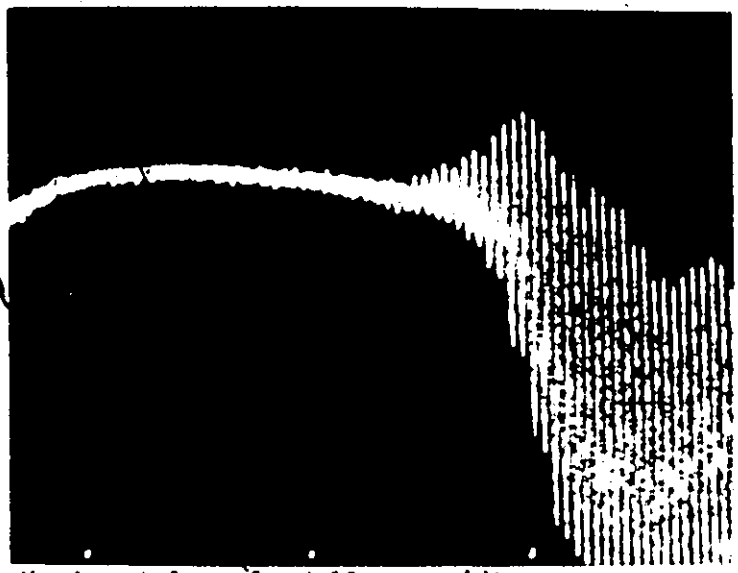

Horizontal scale = 10 nsec /div.

Figure 4.9 b)

Voltage waveforms when the frequency = 980 MHz

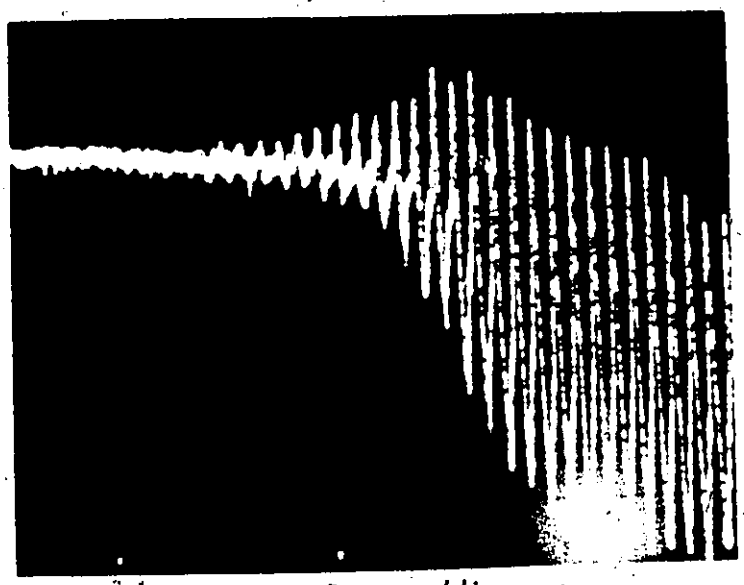

Horizontal scale = 5 nsec /div.
Ampl = Voltage

steady-state is the transition from the small TRAPATT mode into a high efficiency mode which causes the average voltage to decrease.

From the above results, it can be drawn that the first distinguishable oscillation to appear in the TRAPATT waveforms is related to the fundamental frequency. However, the fundamental TRAPATT frequency appears before the mode is completely established.

4.3 The optimum frequency

The analysis of the TRAPATT process by Clorfeinesas applied to the FD-300 by Chaffin shows that its optimum TRAPATT frequency lies between 625 and 700 MHz.

Clorfeine equation related the frequency and the depletion width.

$$f = 0.07 \frac{Vns}{W}$$

where W - depletion width

Vns - saturated electron drift velocity

f - TRAPATT frequency

Inserting the FD-300 parameters (Appendix 2) in the equation, the results is:

$$f = 0.07 \times \frac{10^7 \text{ cm/sec}}{10^{-3}\text{cm}} = 700\text{MHz}$$

Also, in combining two equations derived by Clorfeine, Chaffin has obtained a relation between the frequency and the doping profile

$$f = 0.78 \times 10^{-6} n_d$$

where n_d = n-region doping density (cm^{-3})

Substituting the value of n_d, the frequency becomes:

$$f = (0.78 \times 10^{-6})(8 \times 10^{14}) = 625 \text{ MHz}$$

The period of this frequency corresponds to one cycle of plasma triggering and extraction at twice the critical current density, assuming a rectangular current waveform. Thus, breakdown would occur naturally at this rate provided that sufficient current is delivered promptly by the resonant circuit. The above conditions are closely met in our circuit.

4.4 Conclusion

Inspection of figures 4.4 - 4.9 reveals that in all cases the oscillation starts at a harmonic which is closest to this natural frequency. When the circuit is tuned to 330 MHz (figure 4.4) the growing waveform at the second harmonic is virtually sinusoidal.

Late in the process, higher harmonics grow and shape the signal in the typical TRAPATT fashion. In the circuit tuned for 550 MHz (figure 4.6), the first voltage swings occur at the fundamental frequency which is close to the optimum range. The current waveform reveals that the second harmonic soon triggers a premature breakdown of limited significance until waveshaping enhances the first harmonic again. At 660 MHz (figure 4.7), the rather clean triggering waveform at the fundamental frequency underlines the significance of this frequency as a natural parameter of the device. At 810 MHz (figure 4.8), seizable oscillations occur at the fundamental frequency only. The secondary breakdown is even more limited than at 330 MHz and 550 MHz. This is probably due to the series package inductance L_s, which acts as a low pass filter.

CHAPTER 5

The role of the parasitic components of the diode

5.1 Introduction

In the description of a general circuit model for the TRAPATT mode, Evans has included the diode lead inductance (27). He attributed to this inductance a helpful role in the shaping of the TRAPATT voltage waveform. He did not consider its size as critical.

5.2 The series inductance

Carroll has developed a theory of operation of avalanche diodes in the circuit first analysed by Evans (5,6). Using this theory, Carroll suggested that the package parasitic inductance plays an important role in giving clean triggering waveforms. He also found that for a good operation the size of the inductance must be within 20% of a suitable value which depends on the total capacity at the diode and on the delay of the avalanche in the diode.

The lead inductance of the diode acts as a low pass filter which assignes the respective contribution of each TRAPATT harmonics to the overal waveform. If the inductance is too big, the highest harmonics are attenuated causing a decrease in the triggering pulse amplitude and an enhancement of the

lowest harmonics (fig. 5.1). On the other hand, if the inductance is too small, the presence of large high frequency harmonics produces ringing in the voltage (fig. 5.1). In both cases, the final result is the same, the efficiency of the mode is considerably decreased. It is therefore believed that a small amount of inductance is beneficial to the TRAPATT oscillation.

This theory was verified simultaneously in two circuits, in Evans' circuit and in Chudobiak's microstrip circuit. The experiment was performed as described below.

The diodes were chosen among a hundred because of their electrical similitudes. Among the compared characteristics are the breakdown voltage, the punch through capacitance to breakdown capacitance ratio and the maximum power at the test frequency.

The packaged diode was mounted in both circuits. All the experiments were carried out at 700 MHz. The circuit was tuned for maximum power and the current was maintained at 1.5 amperes in all cases. The output power was measured through a bandpass filter. The bandwidth of the filter was 50 MHz (figure 5.2) so that if the circuit was properly tuned, all the power of the fundamental oscillation fell inside the passband. Except for the first set of results, the ON voltage and its duration were noted in order to evaluate the

Figure 5.1

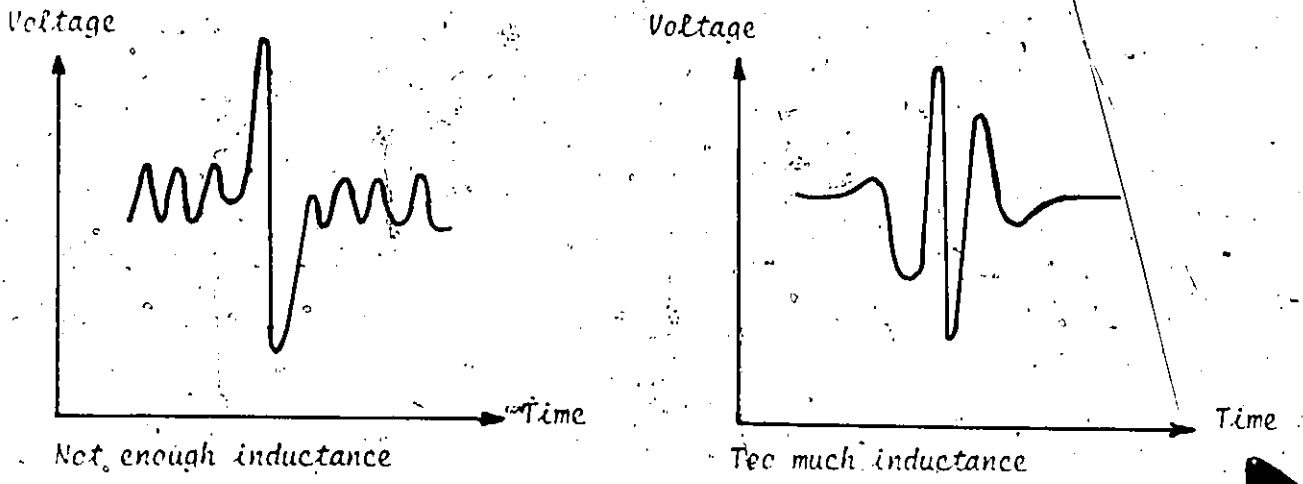

Figure 5.2

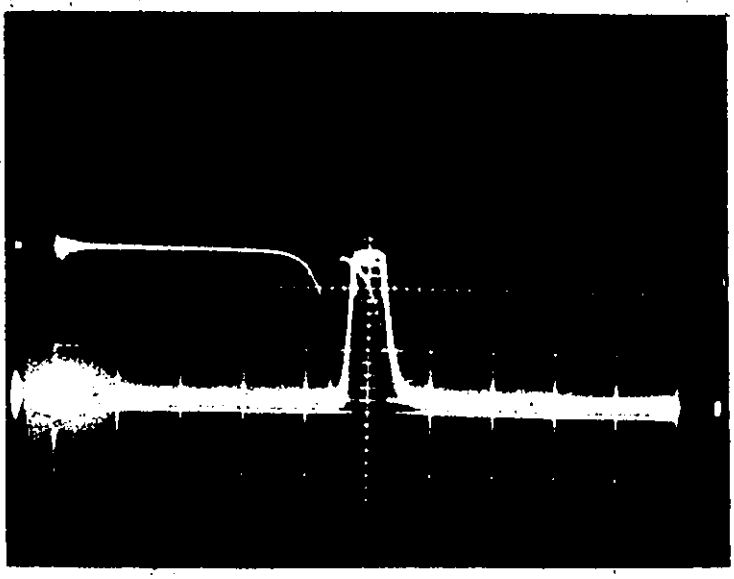

Centre freq = 1.5 GHz
Width = 100 MHz /div.

Insertion loss 1 db

Tunable bandpass filter used to measure the output power of the oscillator.

peak pulse power and the efficiency of the diode.

$$P_p = \frac{P_{av}\, T}{t_{on}} \quad \text{in watts}$$

Where P_p is the peak power

P_{av} is the average power

T is the period of the pulse (1/PRF)

t_{on} is the RF envelope width or the time that the circuit is in the TRAPATT mode.

The same experiment was repeated for the unpackaged diode with the least possible inductance and, after, with some inductance as shown in figures 5.3. The figures 5.4 show the average voltage and current of the packaged and unpackaged diode mounted successively on a microstrip and in an air-line circuit. The tables 5.1, 5.2 and 5.3 are the results obtained in the experiment described above.

In the tables, many spaces were left blank. The reasons are that the small dimensions of the unpackaged diode made it difficult to mount the diode, to make good contact and to avoid arcing.

The experiment was carried further in the microstrip circuit because it is easier to work with this circuit. The length of the inductor was varied to see its effect on the performance of the oscillator. The results are tabulated in table 5.4. In comparison

Figure 5.3 b) *AIR-LINE CIRCUIT TO HOLD THE UNPACKAGED DIODE*

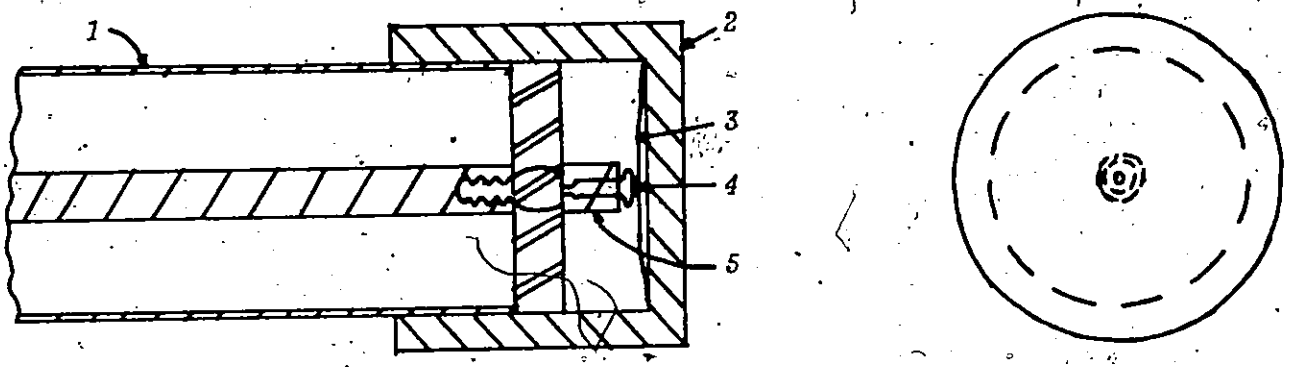

1. *G.R. air-line with the outside connector removed at the end*
2. *Moveable short-circuit termination*
3. *Cooked beryllium-copper*
4. *Diode and diode chip*
5. *G.R. inside connector filled with tin solder*

* *To avoid crown effect and arcing a thin film of silicon compound was spread on the beryllium copper*

Figure 5.3 a) *MICROSTRIP CIRCUIT TO HOLD THE UNPACKAGED DIODE*

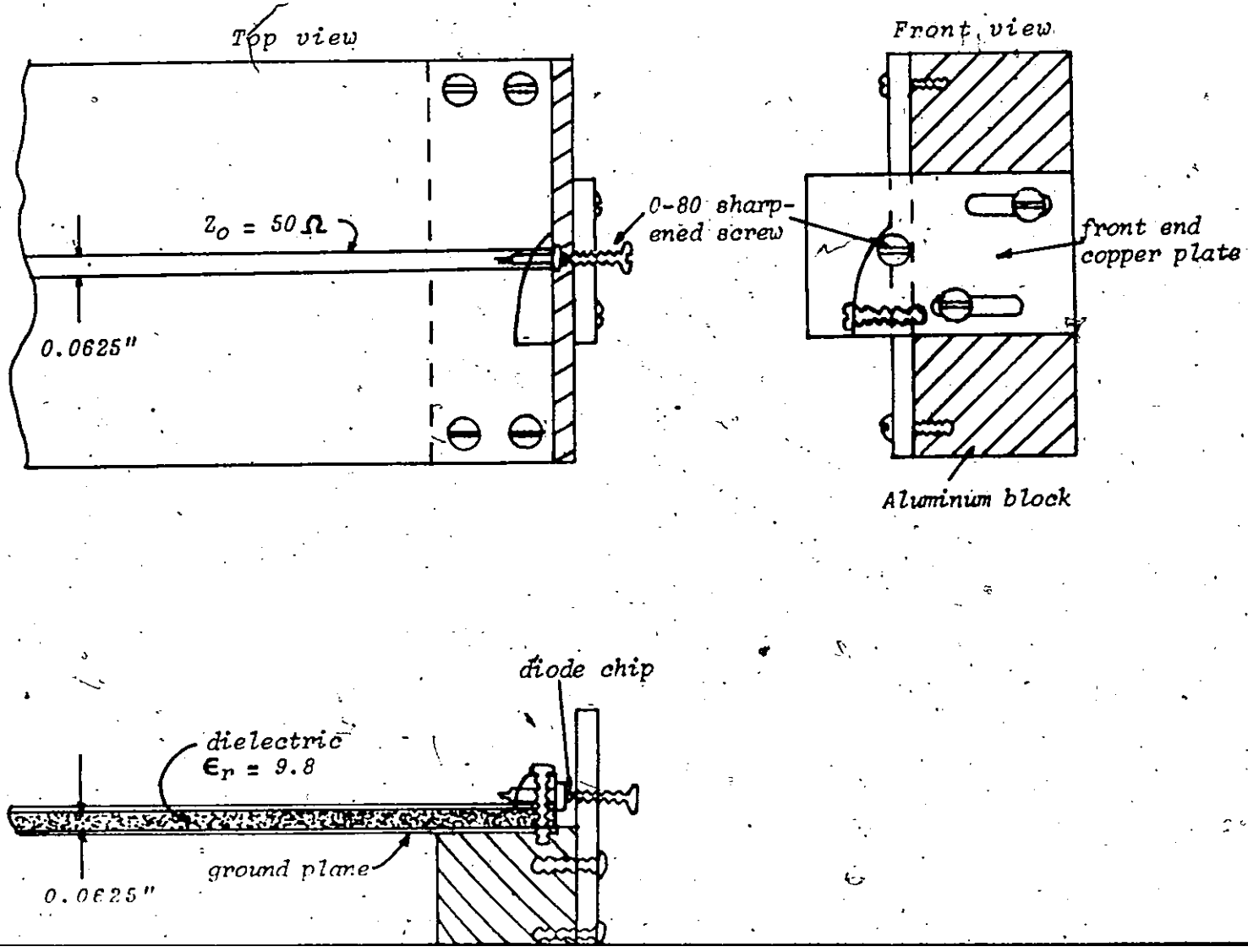

Figure 5.4

The average voltage and current when the inductance is varied. Frequency is kept at 700 MHz

a)

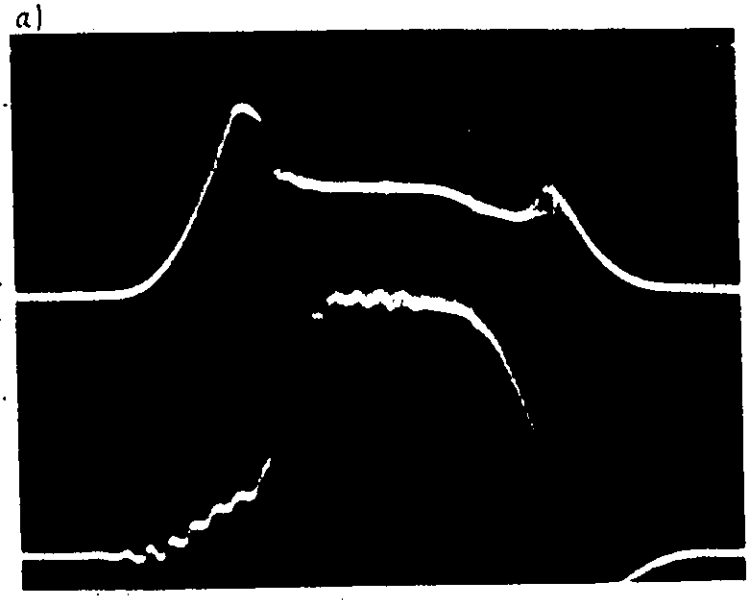

← Voltage - 100 volts /div.

← Current - 0.5 amp. /div.
Horizontal scale= 100 nsec/div.

Packaged Diode mounted in an air-line

Mean power = 5.2 mw
Efficiency = 15 %

b)

Packaged diode mounted on a microstrip

Voltage (top) = 100 volts /div.
Current (Bot.)= 0.5 amp /div.
Horizontal scale=100 nsec/div.

Mean Power = 4.6 mw
Efficiency = 12 %

The TRAPATT mode starts earlier in the air-line than in the microstrip because the former one has a higher Q and this helps the growing of the oscillations.

Figure 5.4

c)

Unpackaged diode mounted on a microstrip with a small inductance

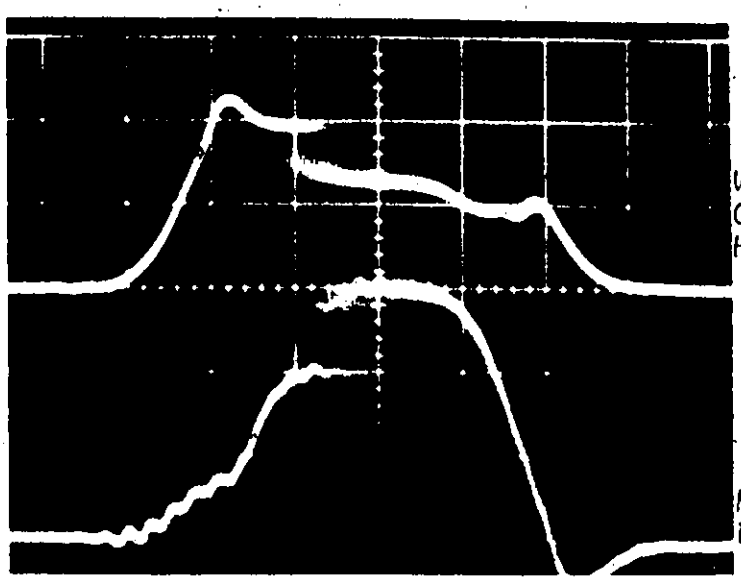

Voltage (top) = 100 volts /div.
Current (bottom)=0.5 amp /div.
Horizontal scale=100 nsec/div.

Mean power = 2.7 mw
Efficiency = 11 %

d)

Unpackaged diode mounted on a microstrip with the less possible inductance

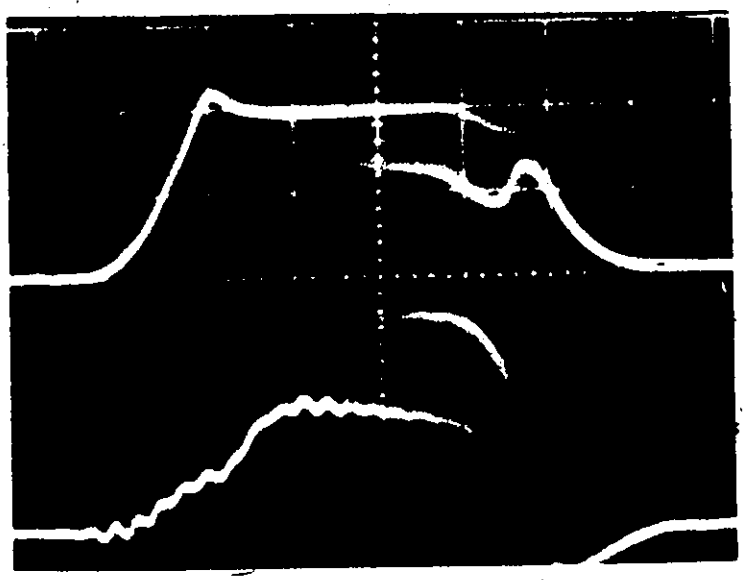

Voltage (top) = 100 volts /div.
Current (bottom)= 0.5 amp /div.
Horizontal scale= 100 nsec/div.

Mean power = 0.8 mw
Efficiency = 5.4 %

This efficiency is meaningless.

This circuit was very hard to start and the output impedance of the pulser had to vary in order to make the diode oscillates.

It is obvious from those pictures that without or with a small inductance, the diode had difficulties to start.

with the package diode output power, the results are similar when the length of the inductor is 0.9 cm.

To further demonstrate the beneficial effect of the diode series inductance, a last experiment was performed. W.J. Chudobiak had noted in his previous experiments that when the unpackaged diode was inserted between the top conductor and the ground plane of a microstrip circuit, it did not oscillate. The experiment was carried out again and the TRAPATT diode did not oscillate. However, when an inductor was installed as shown in figure 5.5, the diode oscillated very well.

Figure 5.5

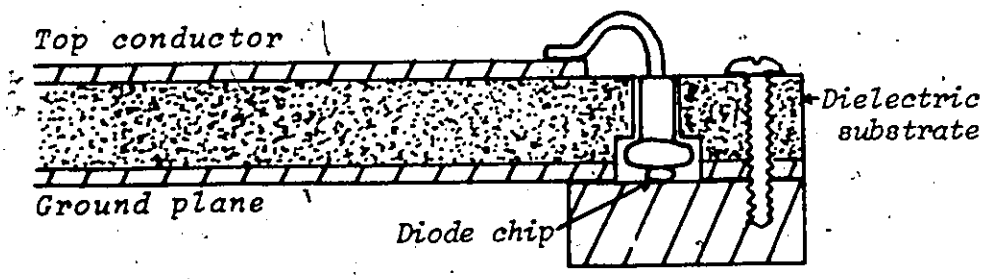

One way in which the inductor can be installed when the diode is held in the microstrip.

When the series inductance is reduced to its minimum, the mean power goes down considerably. This

decrease is mostly due because the TRAPATT mode is not turned on at each pulse. The figures 5.4 compare the biasing voltage and current of the same diode in cases where the inductance is reduced and where the inductive package is present.

5.3 Measurement of the diode impedance

In the above section, it was demonstrated that the presence of an inductance in series with the diode was beneficial if not necessary to the TRAPATT oscillations. Measurements were performed to evaluate this inductance. The diode capacitance has also been measured during the experiment.

The equivalent circuit of the encapsulated diode, biased above breakdown, can be reduced to the circuit shown in figure (5.6) if the resistance are neglected.

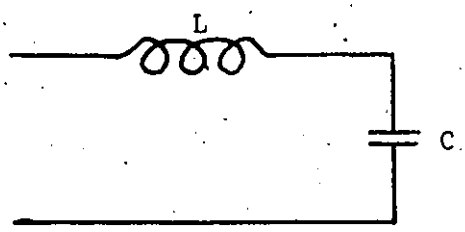

Figure (5.6) Simplified equivalent circuit of the diode

To measure the two components of the simplified equivalent circuit, the following procedures were followed. First, the diode was forward biased

in order to eliminate the junction capacitance C. Then, the inductance L was measured. After, the capacitance was evaluated while the diode was reverse biased at a voltage above breakdown. The experiment has been repeated at many frequencies to detect any dependence of the parameters on frequency.

The inductance and the capacitance where found to be 4 nH and 0.5 pF. Both components show very little dependence on frequency. Those results are in agreement with those obtained by W. Chudobiak (13) and R. Chaffin (7).

The resonant frequency of the junction capacitance in series with the lead inductance is

$$f_o = \frac{1}{2\pi\sqrt{LC}} = \frac{1}{6.28\sqrt{4\times10^{-9}\times5\times10^{-13}}} = 3.9 \text{ MHz}$$

Interesting enough, this is the frequency identified in chapter 2. It can thus be concluded that the small oscillation was caused by this resonant circuit.

5.4 Conclusion

The results of the experiments described in the chapter demonstrated that the efficiency of the TRAPATT oscillation decreases when the lead inductance is eliminated. They also showed that the TRAPATT mode is not triggered at each biasing pulse in the absence of the inductance. It can thus be concluded that a

certain amount of inductance (4 nH) in series with the diode is of double significance: it shapes the TRAPATT waveform and enhances the triggering process.

Table 5.1 (Evan's circuit)

Diode Number	*Packaged P_p in Watts*	*0.15 in inductor P_p in Watts*	*No inductance P_p in Watts*
101	36	4	0
108	34	12	15
127	29	13	8
129	30	20	13
133	30	10	10
135	28		12
146	32	17	12
150	27		*

Table 5.2 (Chudobiak's circuit)

Diode Number	*Packaged P_p in Watts*	*0.15 in inductor P_p in Watts*	*No inductance P_p in Watts*
101	30	22	*
108	28	19	*
127	26		*
129	29	19	15
133	27	22	9
135	27		
146	31	20	1*
150	29	22	

* *Too much unstable to be measured*

The experiment was carried further on microstrip. The length of the inductor was varied to see its effect. The results are tabulated in table 5.4.

Table 5.3

Diode Number	Average power in the microstrip line (mw)			Av. power in air-line (mw)	
	Packaged Diode	Unpackaged li = 0	Unpackaged li = .35cm	Unpackaged li = 0	Unpackaged li = .35cm
48			1.7		
74		1.3	1.6		
80				1.3	2.0
102	4.3		3.3	1.0	
103	4.1			0.7	1.3
110	4.3		3.6		
111	4.2	1.7	3.1	0.6	0.8
112	4.3	2.6	3.2	1.3	1.0
114	4.2		3.9		
116	4.6	0.3	3.0	1.1	1.1
119	3.9	1.5	2.5	1.0	

The above table gives the average power through a bandpass filter, but in the case of the Evan's circuit the tuners used were not giving the maximum power at that frequency.

TABLE 5.4

Diode Number	*Peak pulse power P_p for different lenght li of the inductor (in Watts)*					
	li = 0	*li = 0.15cm*	*li = 0.3cm*	*li = 0.45cm*	*li = 0.9 cm*	*Packaged*
151	16	29	35			27
157	5	12	14	25	29	28
163	5	10	20	24		28
167	*	24	29	35		36
170	*	16	12	26	24	26

CONCLUSION

The experiments and the analysis described in the present study give a clear picture of the physical mechanisms involved in the triggering process of the FD-300 TRAPATT diode.

The triggering behavior has been investigated in the frequency and time domain. The analysis in the frequency domain revealed that the IMPATT oscillation plays no important role in the triggering of the FD-300 oscillator. A small spectral component in the vicinity of 4 GHz which has been observed at the onset of the oscillation was attributed to the resonance of the junction capacitance and parasitic series inductance. This is rather surprising since many authors have considered the presence of IMPATT oscillation to be a necessary condition for the triggering of the TRAPATT mode.

The measurements in the time domain showed clearly that for any tuning in the TRAPATT range of the FD-300 diode, the circuit always starts to oscillate at the particular harmonic which is closest to 660 MHz. Thus, an oscillator tuned to 350 MHz could start to oscillate at 700 MHz before switching to the fundamental frequency. Above 500 MHz, the oscillation would always start at the fundamental frequency.

There are two reasons for this:

- the frequency of 660 MHz is the natural TRAPATT frequency for the diode, i.e. the period of that frequency corresponds to one cycle of plasma triggering and extraction at twice the critical current density
- the series inductance of the package acts as a low pass filter which prevents higher harmonics to trigger premature avalanche during the recovery phase of the diode.

Furthermore, it has been observed during all the experiments that the tuning for maximum output power and efficiency provided the cleanest possible triggering waveforms. This phenomena underlines the importance of the triggering process in a pulsed TRAPATT oscillator. Thus, in the design of an oscillator with a FD-300 diode, the following two conditions must be fulfilled:

- the resonant TRAPATT circuit must support oscillation in the vicinity of the natural frequency of the diode
- the inductance must be provided in series with the diode to form a low-pass filter with cut-off frequency slightly above the natural frequency of 660 MHz.

APPENDIX I

The FD-300 TRAPATT diode

All experiments reported in this paper were carried out using a low cost, commercially available computer diode (FD-300). This p^+-n-n^+ structure (silicon) is capable of oscillating in the pulsed TRAPATT mode at a frequencies ranging from about 250 MHz to 1.5 GHz, figure I.1 shows the doping profile of the diode.

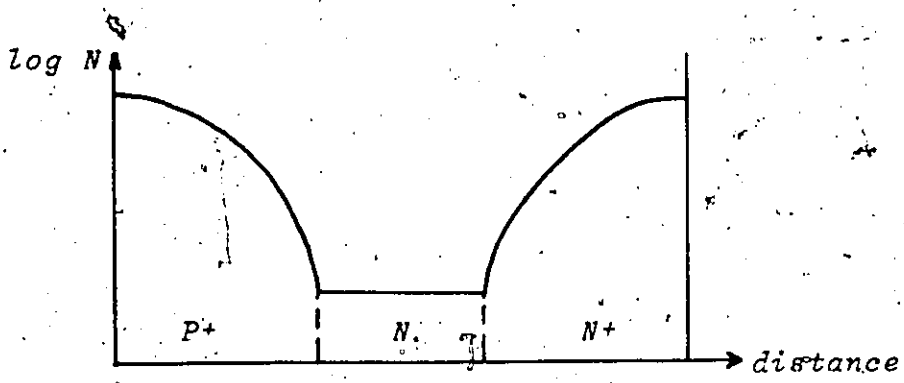

Figure I.1: Doping density profile for TRAPATT oscillator diode

To obtain TRAPATT oscillations, the lightly doped epitaxial region must be fully depleted at a voltage less than the breakdown voltage. The efficiency of the mode is increased when the layer is swept out at about one-half the breakdown voltage or less (punch through voltage = 0.5 breakdown voltage) (15).

Table I.1 summarizes the essential parameters of a typical FD-300 diode.

Table I.1 Parameters of a typical FD-300 TRAPATT diode (After Chudobiak (13) and Chaffin (7))

Depletion width (at breakdown) (W_c)	10 um
Doping concentration in the n-region (N_d)	$10^{15}/cm^3$
Junction diameter (D_j)	210 µm
Static breakdown voltage (V_B)	230 V
Punch-through voltage (V_p)	— 60 V
Saturation current I_s (25° C, 10V reverse bias)	50×10^{-12} A
Thermal resistance (R_{jc})	100° C/Watt
Package series inductance (L_s)	— 4 nH
Junction capacitance C_j (below breakdown)	— 0.4pF

Peak power levels approach 100 Watts in the effective frequency range.

APPENDIX II

Basic principles of TRAPATT operation

When the TRAPATT diode is biased near breakdown, the electric field has the profile of figure (II.1). If the biasing voltage is suddenly increased, the field will momentarily exceed the breakdown value because avalanching does not occur instantaneously. The resulting overvoltage rises the field above the critical value so fast that the avalanche front (point P_a) moves in the diode with a velocity v exceeding the scattering

Figure II.1: Field distribution in the diode as a function of the distance in the junction

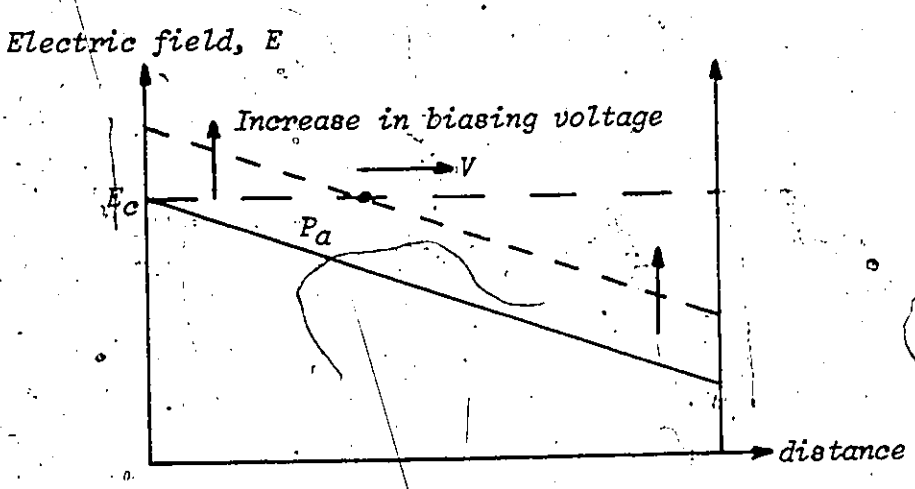

P_a *represents the avalanche front*

--- *field as it should be if no avalanche occurs*

—— *field when the voltage is below the breakdown value*

limited drift velocity of the carriers. Also, as in any avalanche process, a multiplication of carriers occurs wherever the field exceeds the critical value. This causes the field behind the avalanche front to collapse and a large number of majority carriers to be trapped in the low electric field region. Finally, the voltage across the diode falls to nearly zero and a dense plasma fills the junction. The terminal current slowly removes the plasma, and the voltage recovers to the breakdown value.

Once the TRAPATT mode is started, a resonant circuit provides the required triggering pulse at each cycle. This circuit is essentially a transmission line terminated by a low pass filter acting as a short-circuit for all frequencies above the fundamental TRAPATT frequency. The voltage drop at the diode terminals causes a negative impulse to travel towards the filter. After reflection, the impulse is inverted, and it rises the voltage on the line to about twice the breakdown value. At its incidence at the diode, this overvoltage triggers a new avalanche, and the cycle repeates itself. The oscillation frequency is thus almost determined by the electrical distance between the diode and the filter. The resulting voltage and current waveforms are shown in figure II.2.

Figure II.2: Diode voltage and current waveforms

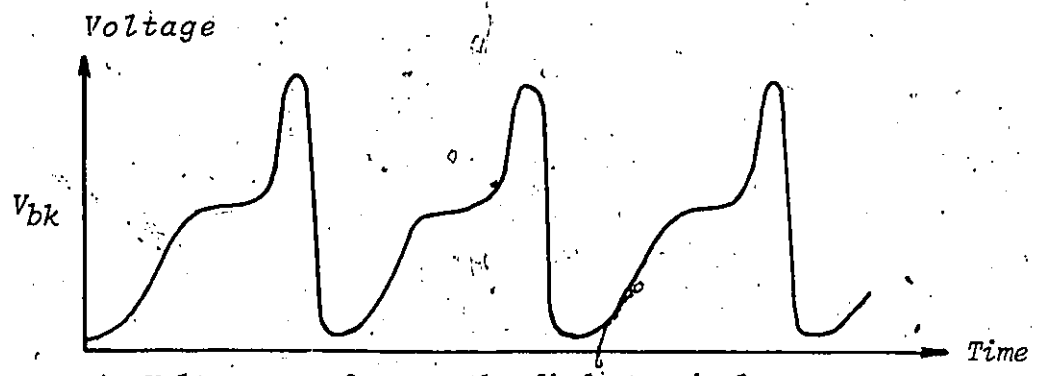

a) Voltage waveform at the diode terminals

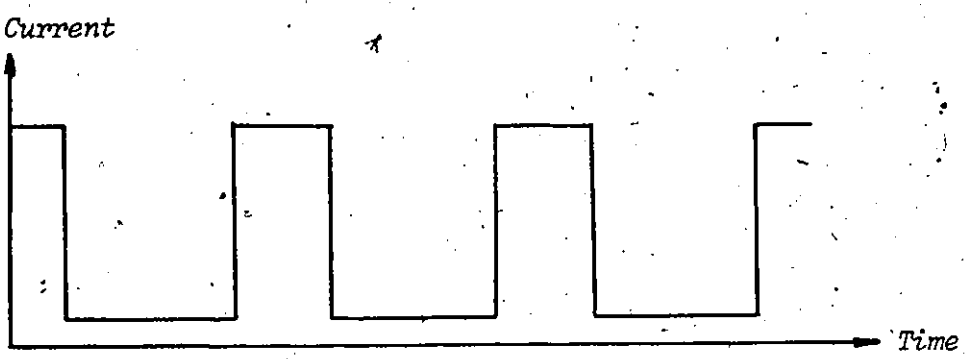

b) Current waveform at the diode terminals

Their similitude with actual voltage and current waveforms can be seen in comparing with figures II.3.

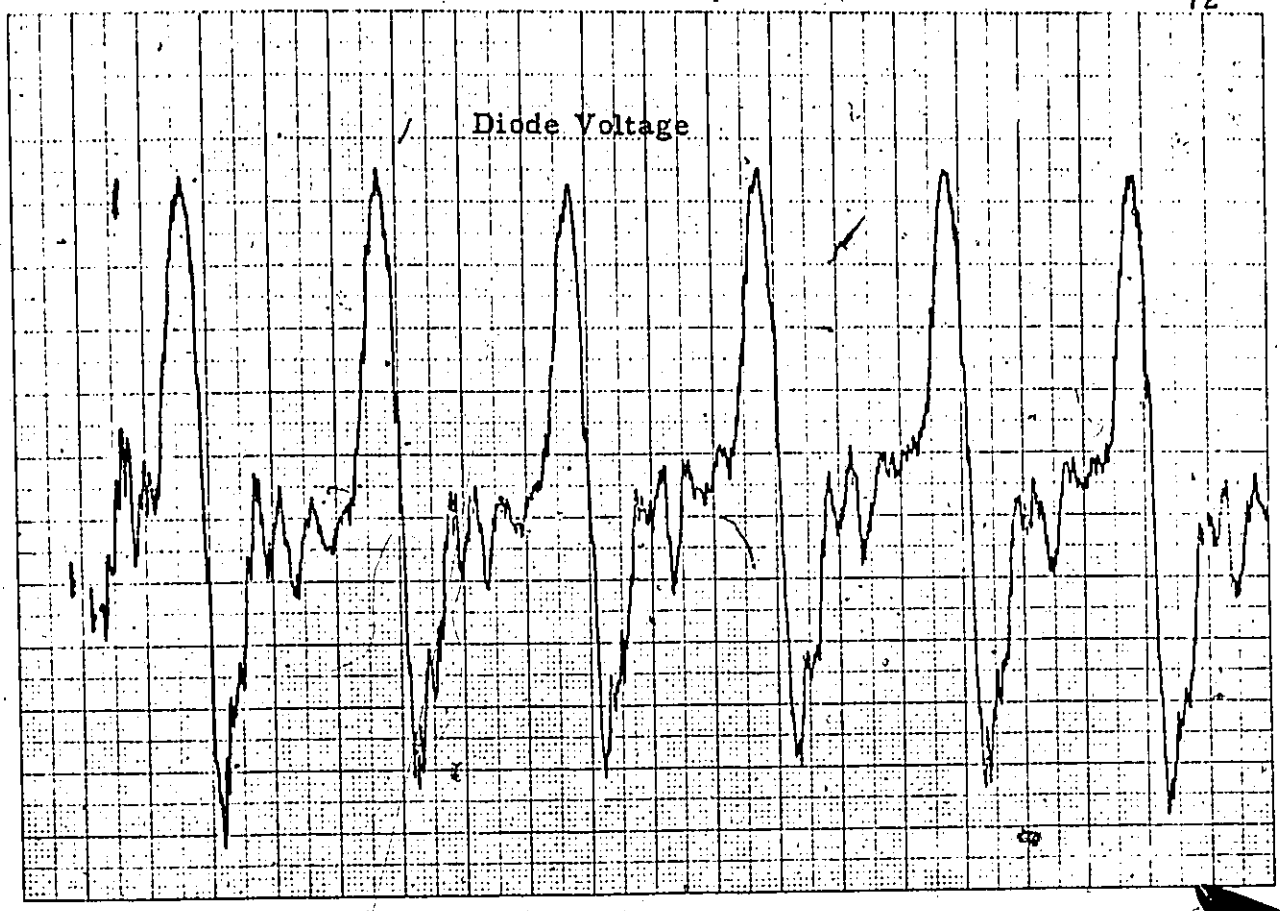

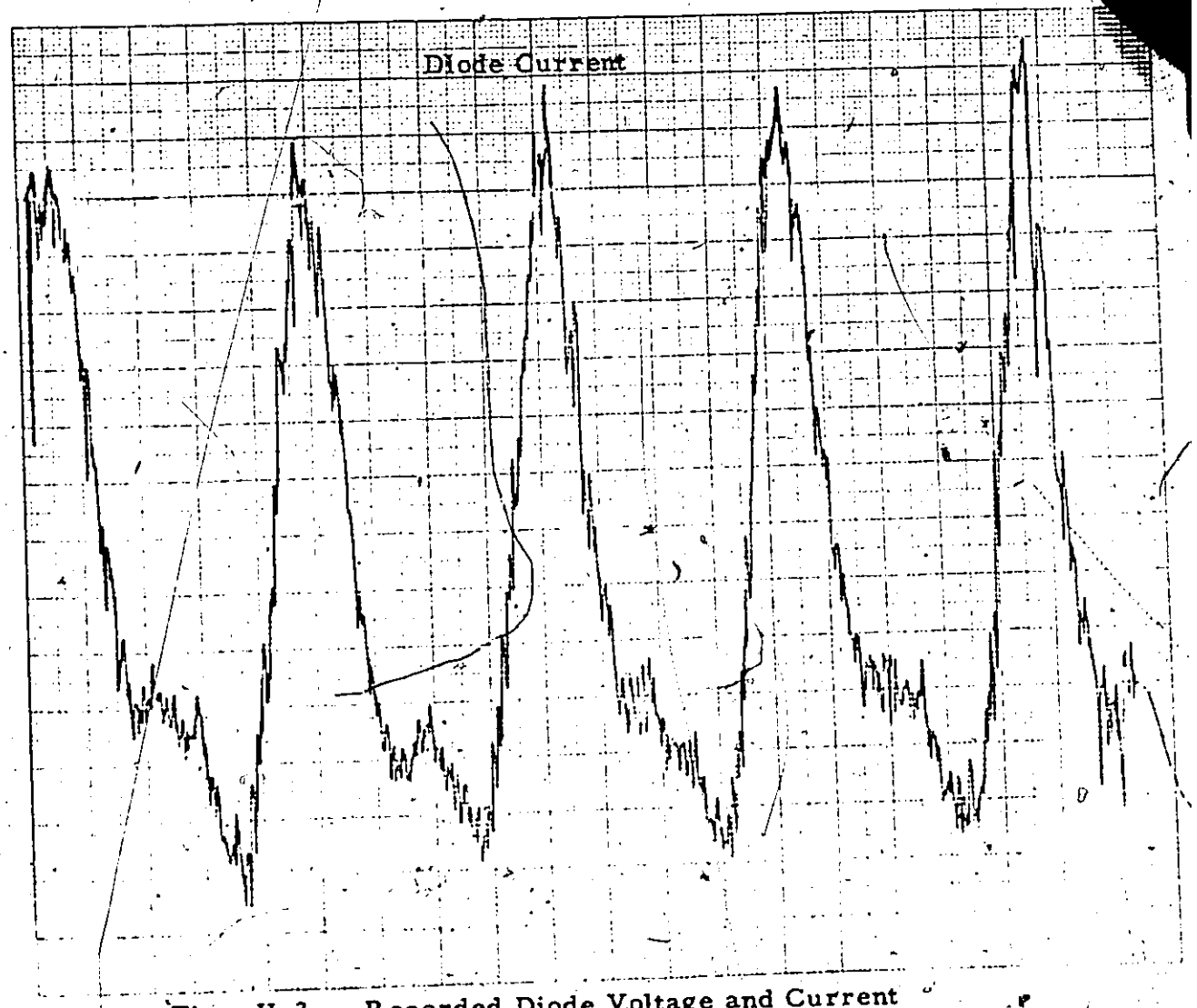

Fig. II.3 Recorded Diode Voltage and Current

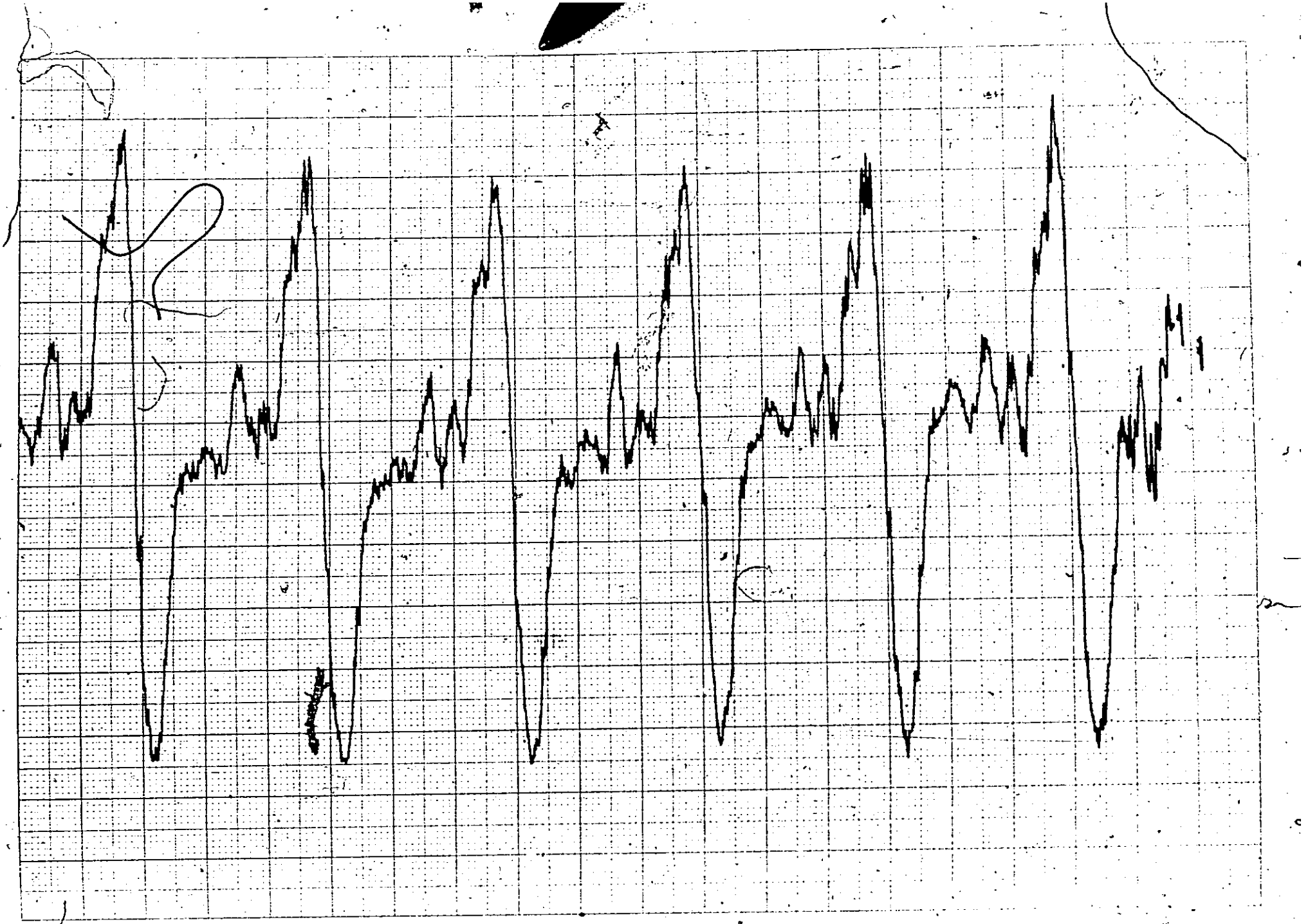

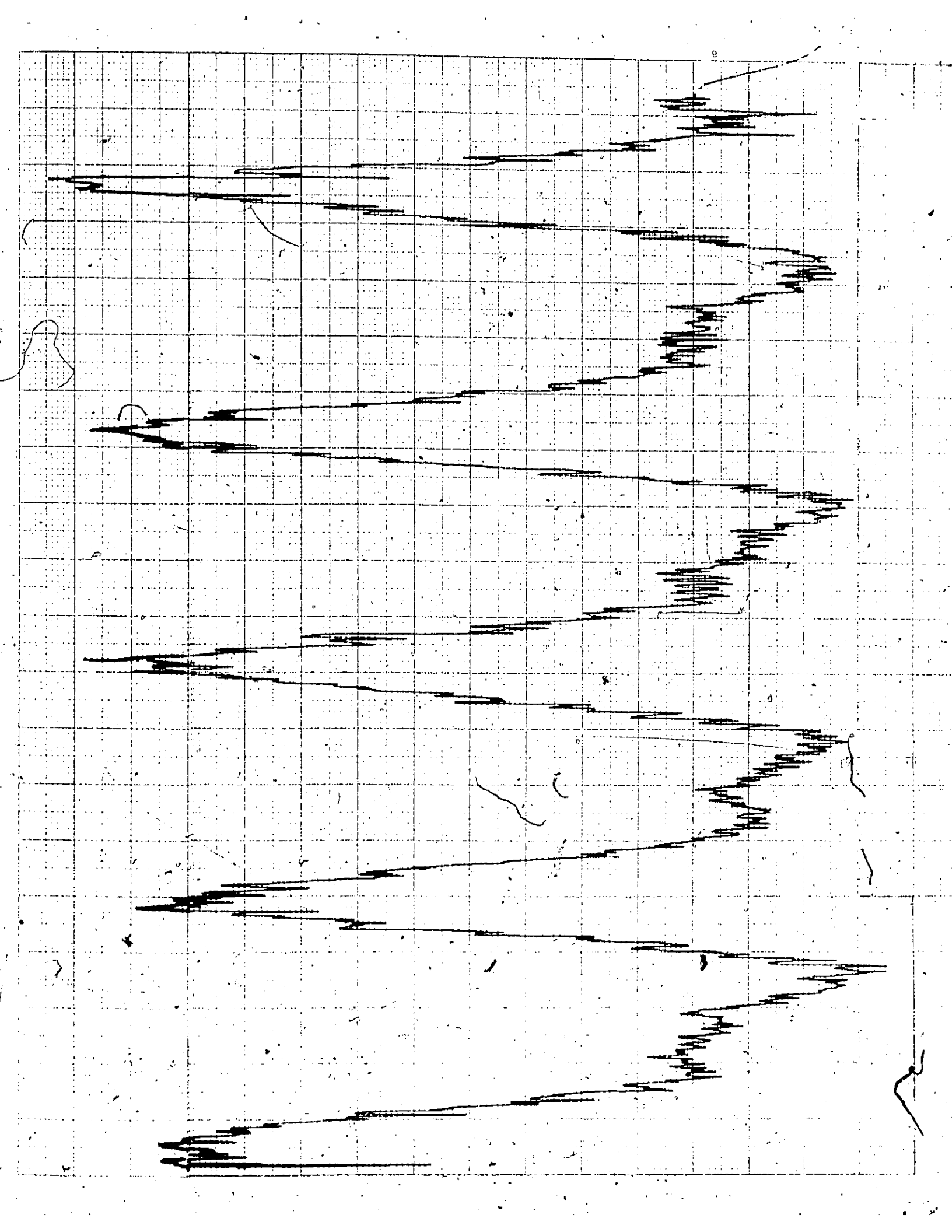

APPENDIX III

Microstrip Wheeler's equations

Calculation of the characteristic impedance of microstrip to calculate the characteristic impedance of a microstrip, one can use Wheeler's equation.

For a narrow strip

$$Z_c = \frac{Z_o}{2\pi\sqrt{k_a}}\left[\ln\left(\frac{8}{W/h}\right)+\frac{(W/h)^2}{32}+1/2\left(\frac{k-1}{k+1}\right)\left(\ln\frac{\pi}{2}-\frac{1}{k}\ln\frac{4}{\pi}\right)\right]$$

k_a $= e^{-(k-1)/2}$

k is the relative dielectric constant

Z_c is the characteristic impedance of the line in ohm

Z_o = 377 ohm

W = width of the strip

h is the thickness of the substrate

For a wide strip

$$Z_c = \frac{Z_o}{k}\left\{\frac{W}{h}+0.882+\frac{k+1}{\pi k}\left[\ln\left(0.5\frac{W}{h}+0.94\right)+1.451\right]+\frac{k-1}{k^2}\times 0.164\right\}^{-1}$$

In any cases

$$\frac{\lambda o}{\lambda m} = \frac{Z_o\ (1, W/h)}{Z_o\ (k, W/h)}$$

λ_o is the free-space wavelength

λ_m is the wavelength in the dielectric

The values of characteristic impedance and of the wavelength ratio are plotted in function of the W/h ratio for several relative dielectric constants in figures III.1.

Figure III.1

RATIO OF FREE SPACE WAVELENGTH (λ_o) TO MICROSTRIP WAVELENGTH (λ_m)
CALCULATED FROM WORK OF WHEELER

WIDE STRIP APPROXIMATION (W/H > .1)

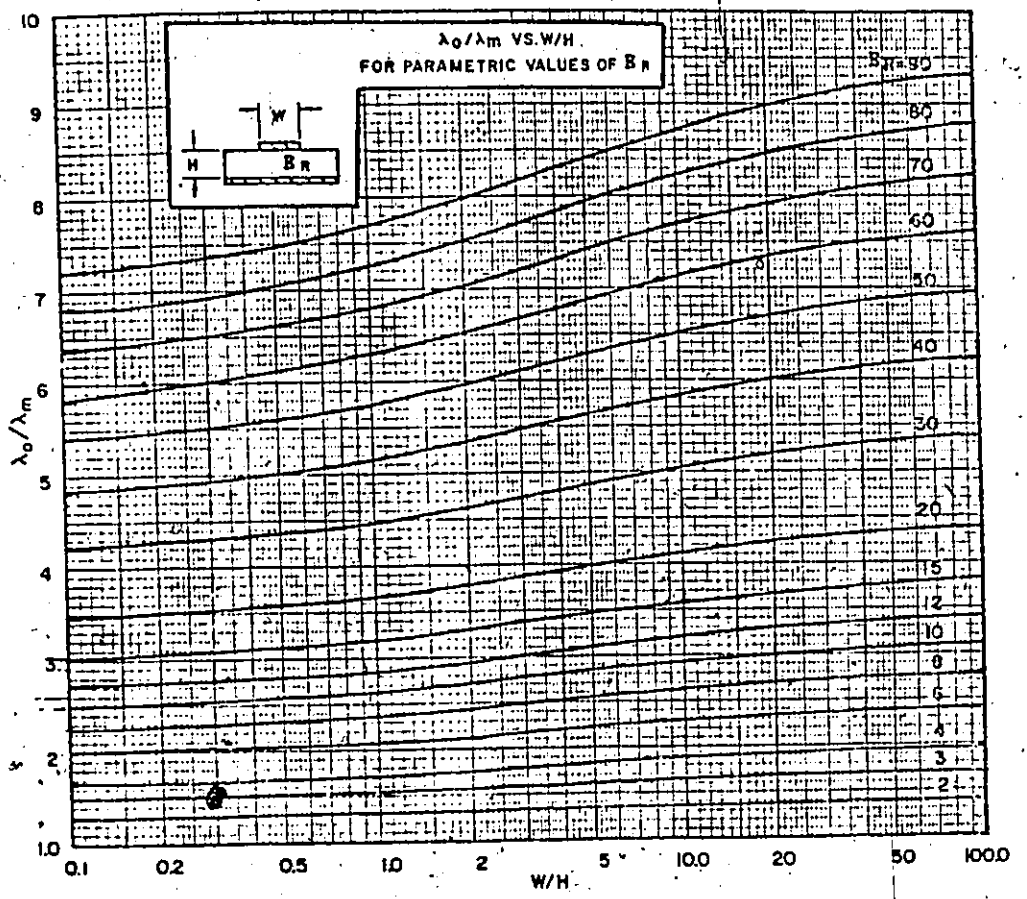

NARROW STRIP APPROXIMATION (W/H < 1.0)

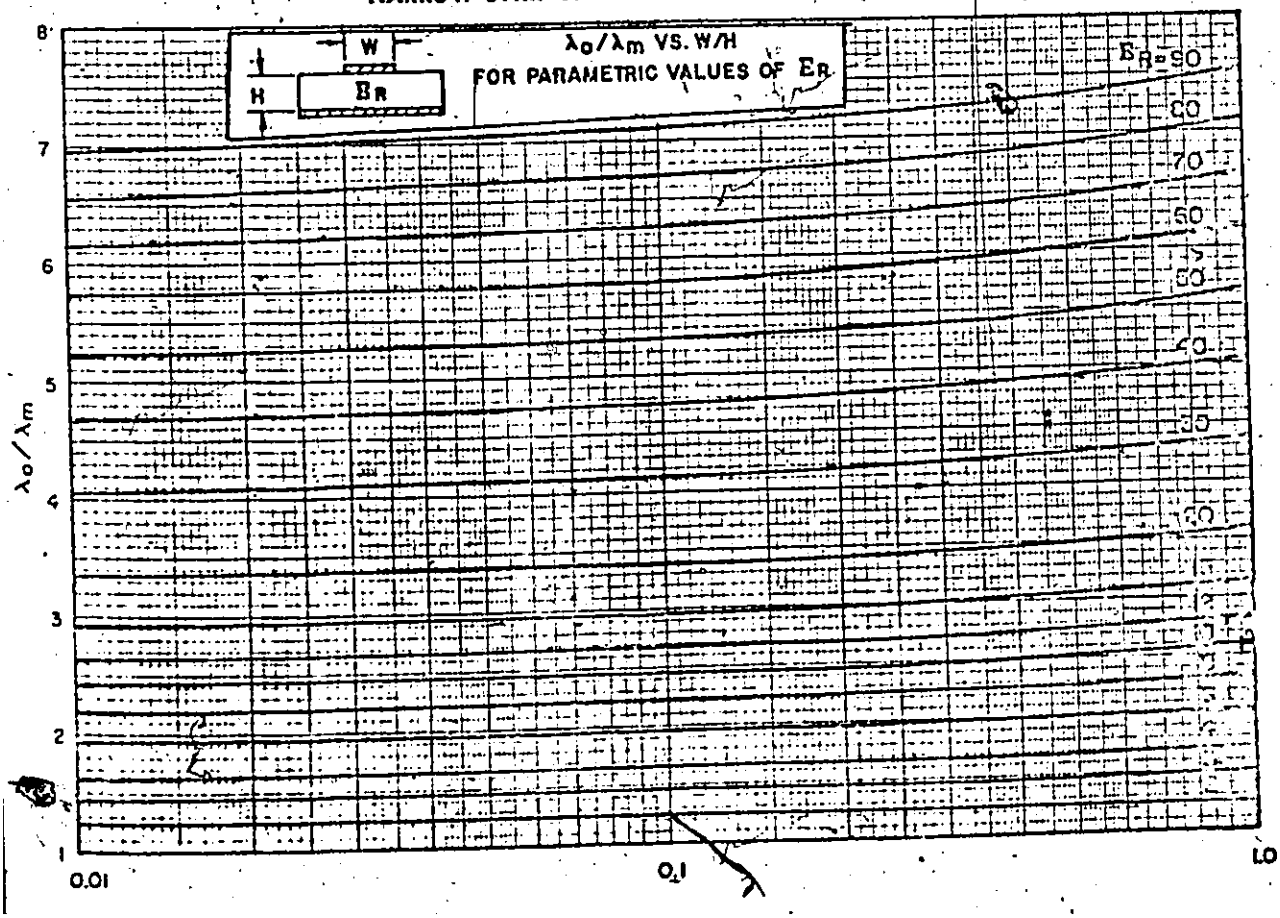

Figure III.1 (con't)

MICROSTRIP CHARACTERISTIC IMPEDANCE CALCULATED FROM WORK OF WHEELER

WIDE STRIP APPROXIMATION (W/H > .1)

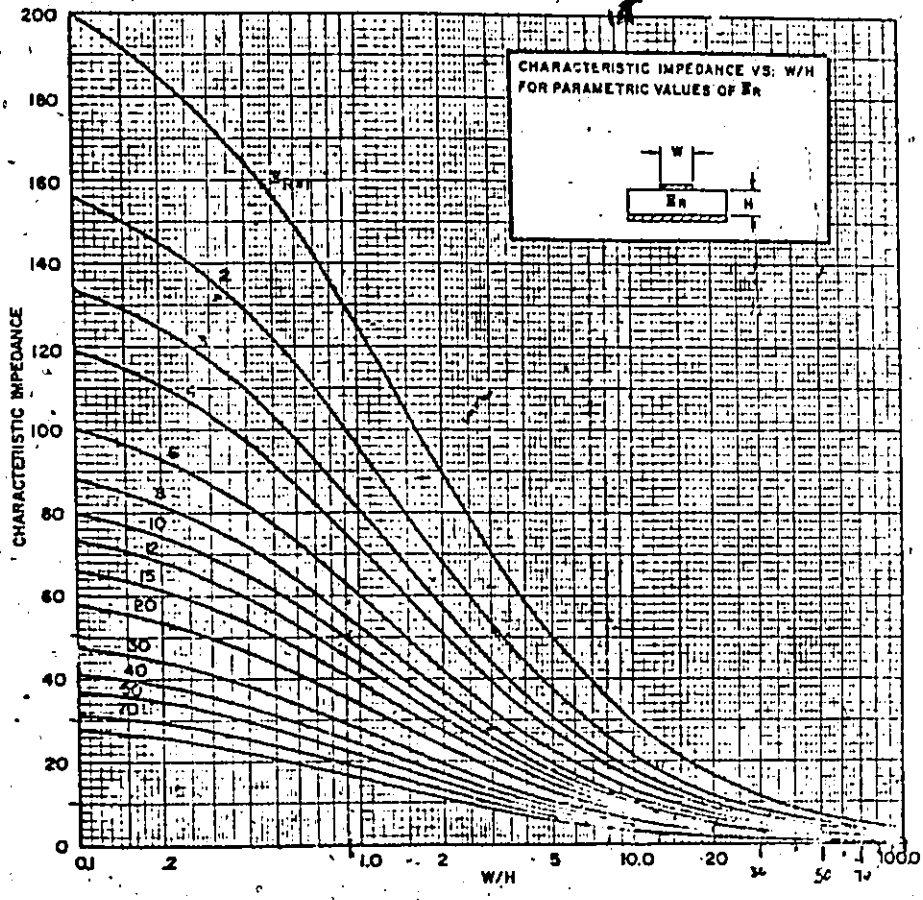

NARROW STRIP APPROXIMATION (W/H < 1.0)

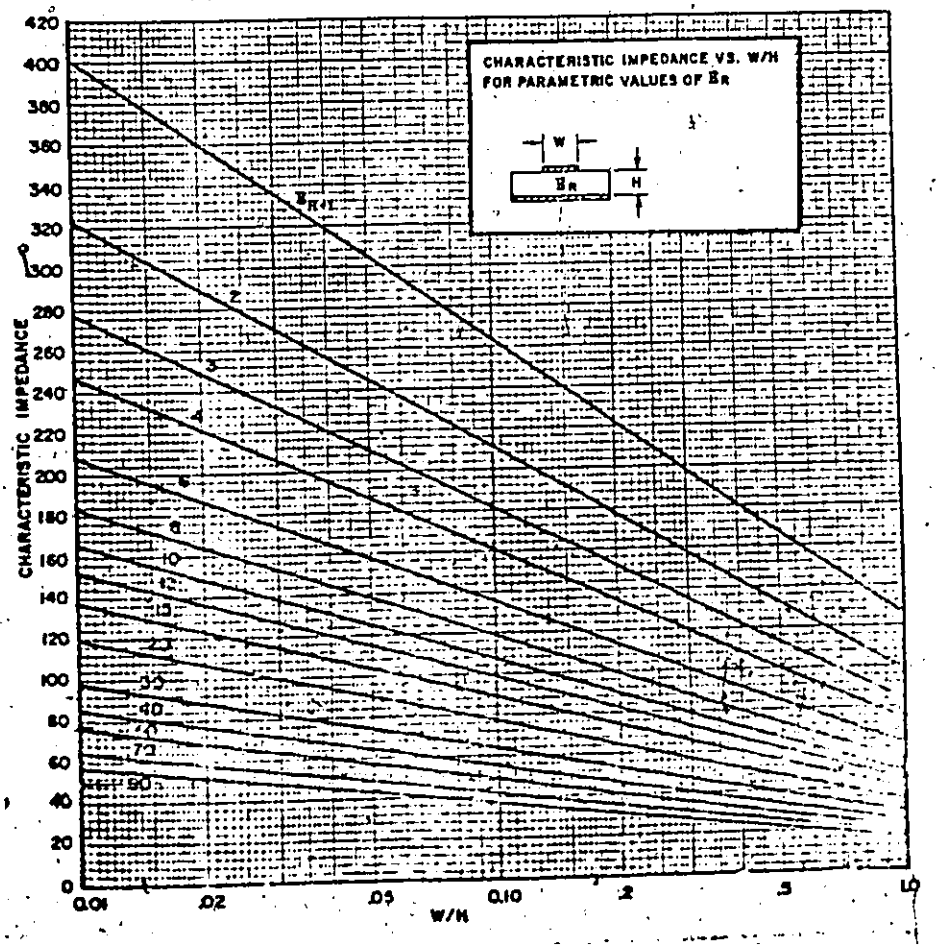

References (TRAPATT)

1 Assour, J.M., 'Impurity Distribution in High-Efficiency Silicon Avalanche Diode Oscillators'. IEEE Trans., Vol. ED-17 No. 10, October 1970, pp. 878-882

2 Bartelink, D.J., and Scharfetter, D.L., 'Avalanche Shock Fronts in p-n Junctions'. Applied Physics Letters, 15 May 1969, Vol. 14, No. 10, pp. 320-323

3 Caroll, J.E., 'The use of Negative Inductance and Related Concepts in the Synthesis of TRAPATT circuits'. 1971 European Microwave Conference, A8/4:1-A8/4:4

4 Caroll, J.E., 'The use of pseudo-transients in the Solution of the Evans TRAPATT Circuits'. Proc. 1971 European Microwave Conference A8/4:1 - A8/4:4

5 Caroll, J.E., and Credé, R.H., 'A computer simulation of TRAPATT Circuits'. Int. J. of Electron, 1972, Vol. 32, No. 3, pp. 273-296

6 Caroll, J.E., 'An Analytic Theory for the Evans circuits for avalanche Diodes'. IEEE Trans., Nov. 1970, MTT-18, pp. 977-979

7 Chaffin, R.J., and Nisse, Eer, 'A Poor Man's TRAPATT Oscillator'. Proc. Inst. Elect. Engr., 1970, 58, pp. 173-174

8 Chaffin, R.J., 'High Power TRAPATT Oscillations from Parallel-Connected Low Cost Diodes'. IEEE Trans. Vol. MTT-18, No. 11, Nov. 1970, pp. 985-986

9 Chaffin, R.J., 'A Proposed Circuit model for Microstripline TRAPATT Oscillators'. IEEE Trans. Vol. MTT-18, No. 11, Nov. 1970, pp. 983-985

10 Chaffin, R.J., 'Temperature Dependence of TRAPATT Oscillators'. Proc. IEEE, August 1971, pp. 1270-1271

11 Chang, K.K.N., 'Avalanche Diodes as UHF and L-Band Sources'. RCA Review pp. 3-14, March 1969.

12 Chudobiak, W.J., 'TRAPATT Microstrip Oscillator'. International Electronic Conference, Toronto, October 1971.

13 Chudobiak, W.J., 'TRAPATT Microstrip Oscillator'. Electronics Letters, July 1970, Vol. 6, No. 14, pp. 438-439.

14 Chudobiak, W.J., and Burill, R.P., 'A Low-Cost, High-voltage, Solid-State, TRAPATT Diode Pulses'. Notes and Experimental Technique and Apparatus, 1971, pp. 784-786

15 Clorfeine, A.S., Ikola, R.V., and Napoli, L.S., 'A theory for the High-Efficiency mode of Oscillation in avalanche Diodes'. RCA Review, 1969, 30, pp. 397-471

16 Cottam, M.G., 'Theory for Power Output and Efficiency of Silicon TRAPATT Oscillators'. Elec. Letters 11th June 1970, Vol. 6, No. 12, pp. 384-385

17 Cottam, M.G., 'Theory for High-Efficiency Oscillations in Silicon Avalanche Diodes'. Elec. Letters 2nd April 1970, Vol. 6, No. 7, pp. 203-205

18 Culshaw, B., 'Low-Frequency operation of Avalanche Diodes Under Large-Signal Conditions'. Elec. Letters 13th Nov. 1969, No. 23, Vol. 5, pp. 583-585

19 Culshaw, B., 'Time-Domain Model of the Device/Circuit Characteristics of a Trapped plasma mode Avalanche-Diode Oscillator'. Elec. Letters 17th June 1971, Vol. 7, No. 19, pp. 339-340

20 Culshaw, B., 'High Efficiency Low Frequency Operating Modes in Avalanche Diodes under Low Current Densigy Conditions'. Proc. IEEE Vol. 117, No. 12, pp. 2221-2227

21 Craig, Pletcher, Snapp, 'Experiments on the Nature and Capabilities of Trapped Plasma Mode Harmonic Generation'. 1971 European Microwave Conference, A8/2:1 - A8/2:4

22 Davidson, B.J., White, P.M., Gibbons, G., and Eddolls, D.V., 'Operation and Characterisation of TRAPATT mode Gallium Arsenide Avalanche Oscillators'.

23 De Boise, R.H., and Shackle, P.W., 'C.W. Anomalous Mode Operation in Silicon Planar IMPATT Diodes'. Elec. Letters 29th May 1969, Vol.5, No. 11, pp. 232-233

24 Deloach, B.C., and Scharfetter, D.L., 'Device Physics of TRAPATT Oscillators'. IEEE Trans. 1970, ED-17, pp. 9-21

25 Deloach, B.C., Member IEEE, and Johnston, R.L., 'Avalanche Transit-Time Microwave Oscillators and Amplifiers'. IEEE Trans. Elec. Devices January 1966, pp. 181-186, Vol. ED-13 No. 1

26 Dienst, J.F., D'Aiello, R.V., and Thomas, E.E., 'Power Amplification Using and Avalanche Diode'. Elec. Letters 10th July 1969, Vol. 5, No. 14, pp. 308-309

27 Evans, W.J., 'Circuits for High-Efficiency Avalanche Diode Oscillators'. IEEE Trans., Vol. MTT-17, No 12, Dec. 1969

28 Evans, W.J., Johnston, R.L., 'Improved performance of CW Silicon TRAPATT Oscillators'. Proc. Letters IEEE, May 1970, pp. 845-846.

29 Evans, W.J., 'CW TRAPATT Amplification'. IEEE Trans. Vol. MTT-18, No. 11, November 1970, pp. 986-988

30 Evans, W.J., 'Computer Experiments on TRAPATT Diodes,' IEEE Trans. Vol. MTT-18, No. 11, Nov. 1970, pp. 862-871

31 Evans, W.J., and Iglesias, D.E., 'CW Silicon TRAPATT Operation'. Proc. Letters Feb. 1970, pp. 285-286

32 Franklin, Peter, "Editor", 'Why High Efficiency at Avalanche Subharmonics'. Microwave News, April 1969

33 Grace, M.I., and Gibbons, G., 'High Efficiency Microwave Oscillations from Si Avalanche Diodes'. Elec. Letters, 13th Dec. 1968, Vol. 4, No. 25, pp. 264-265

34 Grace, M.I., 'Broad Band High-Efficiency Mode Amplifiers at S Band'. 1971 European Microwave Conference, 'A8/1:1 - A8/1:4

35 Hoefflinger, B., Snapp, C.P., and Stark, L.A., 'High Efficiency Avalanche Resonance Pumped Amplification'. Elec. Letters, 6th Feb. 1969, Vol. 5, No. 3, pp. 43-45

36 Hoefflinger, B., Zappert, F., and Snapp, C.P., 'Simplified Model for Avalanche-Resonance-Pumped Semiconductor Diodes'. Elec. Letters 13th Nov. 1969, Vol. 5, No. 23, pp. 590-592

37 Iglesias, D.E., 'High Efficiency CW IMPATT Operation'. Proc. IEEE September 1968, pp. 1610

38 Jain, O.P. Makios, V., and Chudobiak, W.J., 'The High-Frequency behaviour of Microstrip transmission lines'. Conference

39 Johnston, R.L., and Scharfetter, D.L., 'Low-frequency High-Efficiency Oscillations in Germanium IMPATT Diodes'. IEEE Trans. 1969, ED-16, pp. 905-911

40 Johnston, R.L., Scharfetter, D.L., and Bartelink, D.J., 'High-Efficiency Oscillations in Germanium Avalanche Diodes Below the Transit-Time Frequency'. Proc. Letters IEEE, Sept. 1968, pp. 1611-1613

41 Kerzar, B., Weissglas, P., 'Voltage and Current Waveforms and TRAPATT Oscillator Optimization'. 1971 European Microwave Conference A8/3:1 - A8/3:4

42 Lui, Shing Gong, 'Harmonic Extraction from High Efficiency Avalanche Diodes'. Proc. IEEE Vol. 59, No. 8, August 1971, pp. 1216-1221

43 Lui, Shing Gong, 'A Compact Microstrip, High Power High-Efficiency Avalanche Diode Oscillator'. Trans. IEEE, Vol. MTT-18, No. 11, Nov. 1970, pp. 982-983

44 Lui, Shing Gong, 'Microstrip High Power High-Efficiency Avalanche Diode Oscillator'. IEEE Trans. 1969, MTT-17 pp. 1068-1071

45 MacKintosh, I.W., and Royds, R.J., 'An Analysis of a TRAPATT Oscillator Circuit'. 1971 European Microwave Conference, pp. A9/3:1 - A9/3:4

46 MacKintosh, I.W., and Royds, R.J., 'The Observation of TRAPATT Microwave Oscillator Waveforms'. pp. 4/1 - 4/4

47 Malsumura, M. and Abe, H., 'Computer Simulation of anomalous mode oscillation in Silicon Avalanche Diodes'. IEEE Trans No. 1970, MTT-18, pp. 975-977

48 O'Callaghan, M., Deadman, H.A., and Hambleton, K.G., 'Measurement of D.C. Negative Resistance in Avalanche Diodes and Its relation to Anomalous-Mode Operation'.

49 Penfield, P., ' Proposed High-Efficiency Diode Oscillator'. Elec. Letters 21st August 1969, Vol. 5, No. 17, pp. 387-388

50 Prager, H.U., Chang, K.K.N., and Weisbrod, S., 'High power, High Efficiency Silicon Avalanche Diodes at Ultra High Frequencies'. Proc. IEEE, April 1967, pp. 586-587

51 Prager, H.U., Chang, K.K.N., and Weisbrod, S., 'Power Amplification with Anomalous Avalanche Diodes'. IEEE Trans. 1970, MTT-18, pp. 956-963

52 Pratt, H.J., 'High Efficiency Avalanche Mode in Microstrip'. Elec. Letters 2 nd October 1969, Vol. 5, No. 20, pp. 467-468

53 Rosen, A., and Assour, J., 'Silicon Avalanche Diode Microstrip L-Bnad Oscillator'. IEEE Trans. Vol. Mtt-18, No. 11, Nov. 1970 pp. 979-981

54 Scharfetter, D.L., 'Power-frequency characteristics of the TRAPATT diode mode of High-Efficiency Diodes'. B.S.T.J., May-June 1970, pp. 800-825

55 Scharfetter, D.L., 'Power frequency characteristics of the TRAPATT diode mode of High-Efficiency Power generation in Germanium and Silicon Avalanche Diodes'. The Bell System Technical Journal May-June 1970, pp. 799-825

56 Slaymaker, N.A., and Caroll, J.E., 'Efficiency power Extraction at TRAPATT Harmonics'. Elec. Letters, 12th Nov. Vol. 6, No. 23, pp. 744-746

57 Slaymaker, N.A., and Caroll, J.E., 'Improved Sampling Technique for the observation of high Harmonics in TRAPATT Waveforms'. Elect. Letters, 9th Sept. 1971, Vol. 7, No. 18, pp 554-555

58 Snapp, C.P., 'Subharmonic Generation and the TRAPPED-Plasma Mode in Avalanching Silicon p+-n-n+ Junction'. IEEE Trans. 1971, ED-18, pp. 294-308

59 Snapp, C.P., 'External Current-Waveform Measurements of High-Efficiency oscillation in Silicon Avalanche Diodes'. Elec. Letters 1970, Vol. 6, No. 5, pp. 145-147

60 Thomson, I., 'High Efficiency Continuous Oscillations in Silicon IMPATT diodes below the Transit-Time Frequency'. Elec. Letters 29th May 1969, Vol. 5, No. 11, pp. 229-230

61 Waard de, P.J., 'Anomalous Oscillations with Punch-Through type Avalanche Diodes'. 1971 European Microwave Conference'. pp. A9/1:1 - A9/1:4

62 Watkins, J., 'Circular resonant structures in microstrip'. Elec. Letters, 18 oct. 1969, Vol. 5, No. 31, pp. 524-525

63 Wheeler, H.A., 'Transmission Line Properties of parallel Wide strips by a Conformal-Mapping approximations'. IEEE Trans. Mtt-12 May 1964, p. 280

64 Wierich, Reinhard, L., 'Computer Simulation of the Dependence of TRAPATT oscillations and their noise spectrum on the minority saturation currents'. 1971 European Microwave Conference A9/4:1 - A9/4:4

65 Yanai, H., Torizuka, H., and Yamada, N., 'Large Amplitude High-Efficiency Oscillation using Si-Avalanche Diode and its experimental analysis'. Dept. of Electronic Eng. University of Tokyo